M.Tech (Geoinformatics)

Kamini Sharma

2023

# URBAN FEATURE EXTRACTION USING HYPER-SHARPENING

A DISSERTATION

SUBMITTED IN PARTIAL FULFILMENT OF THE REQUIREMENTS
FOR THE AWARD OF THE DEGREE
OF

MASTER OF TECHNOLOGY
IN

**CIVIL ENGINEERING**
(With Specialization in Geoinformatics Engineering)

Submitted By:

**KAMINI SHARMA**
**(2K21/GEO/02)**

Under the supervision of

DR. (COL.) K.C. TIWARI, PROFESSOR

**MULTIDISCIPLINARY CENTRE FOR GEOINFORMATICS**
**DEPARTMENT OF CIVIL ENGINEERING**
DELHI TECHNOLOGICAL UNIVERSITY
(Formerly Delhi College of Engineering)
Bawana Road, Delhi – 110042

MAY 2023

# URBAN FEATURE EXTRACTION USING HYPER-SHARPENING

A DISSERTATION

SUBMITTED IN PARTIAL FULFILMENT OF THE REQUIREMENTS
FOR THE AWARD OF THE DEGREE
OF

MASTER OF TECHNOLOGY
IN

**CIVIL ENGINEERING**
(With Specialization in Geoinformatics Engineering)

Submitted By:

**KAMINI SHARMA**
**(2K21/GEO/02)**

Under the supervision of

DR. (COL.) K.C. TIWARI, PROFESSOR

**MULTIDISCIPLINARY CENTRE FOR GEOINFORMATICS**
**DEPARTMENT OF CIVIL ENGINEERING**
DELHI TECHNOLOGICAL UNIVERSITY
(Formerly Delhi College of Engineering)
Bawana Road, Delhi – 110042

MAY 2023

## CANDIDATE'S DECLARATION

I, **Kamini Sharma**, Roll No. 2K21/GEO/02 of M.Tech. Geoinformatics, hereby declare that the project dissertation titled "**Urban Feature Extraction Using Hyper-Sharpening**" which is submitted by me to the Department of Civil Engineering, Delhi Technological University, Delhi in partial fulfilment of the requirement for the award of the degree of Master of Technology, is original and not copied from any source without proper citation. This work has not previously formed the basis for the award of any Degree, Diploma, Associateship, Fellowship, or other similar title or recognition.

Place: Delhi **KAMINI SHARMA**

Date:

## CERTIFICATE

I hereby declare that the Project Dissertation titled "**Urban Feature Extraction Using Hyper-Sharpening**" which is submitted by **Kamini Sharma**, Roll No 2K21/GEO/02 [Civil Engineering] Delhi Technological University, Delhi in partial fulfilment of the requirement for the award of the degree of Master in Technology, is a record of the project work carried by the student under my supervision. To the best of my knowledge this work has not been submitted in part or full for any Degree or Diploma to this university or elsewhere.

Place: Delhi

Date:

**Dr. (Col) K.C. TIWARI**

**SUPERVISOR**
Professor, Multidisciplinary Centre for Geoinformatics
Department of Civil Engineering
Delhi Technological University
(Formerly Delhi College of Engineering)
Bawana Road, Delhi – 110042

## ABSTRACT

Satellite data has proven beneficial in quick monitoring of large urban areas and its various features. Urban centres are heart of country and concentrates large population and development so there regular mapping is essential for various applications such as monitoring City's growth, Urban climate, Hydrological changes, Pollution of water and air, Natural disasters, Socio-economic factors. So, satellite data and its products are actually used to make cities more liveable and advance towards sustainability.

This study aims at monitoring some of those crucial urban parameters- Impervious surface area, Pervious surface area and Urban Green space in one of the largest and densely populated cities in the world, Delhi in India. It was done by creating a finer scale LULC generated from a high Spectral-Spatial resolution Hyperspectral Data from PRISMA sensor. The Hyperspectral data was hyper-sharped from 30 m to 5 m spatial resolution using CNMF algorithm. It was then classified into LULC classes Water, Vegetation, Buildings, Roads and Bare land using machine learning algorithm and extracted for the required Urban features for two areas of the city. The maps of Impervious-Pervious surface areas and Urban green space were also created. The Areas of these urban features was also measured. At last, the results were compared with validation samples and higher resolution datasets for the assessment of accuracy. The classification accuracy for this method for two areas in Delhi was observed as 87 and 92%. The areal accuracies for urban features were found in range of 51.4 to 95.3 %.

## ACKNOWLEDGEMENTS

At First, I would l like to express my gratitude towards my Academic supervisor Dr. (Col) K.C. Tiwari, Professor, DTU for his advices, guidance and motivation during the duration of this effort. The freedom and supportive environment he provided us for pursuing our research was very encouraging for us.

I want to thank my Mother, Father and Brother for providing me all the necessary support and care so I could pursue my work comfortably.

I am indebted to the persistence support received from all the faculty members of The Multidisciplinary Centre for Geoinformatics, Delhi Technological University, who have provided me right knowledge that helped me to complete my research and degree successfully. I would like to recognize the invaluable assistance obtained from my fellow batch mates, Gaurav, Vidit, Aadil and Ewaz during my course over all these months.

I would also like to thank our senior Sushmita Gautam, JRF, DGRE for her advices and technical support.

I would also like to thank Mr. Kaustubh Ranjan Singh, Assistant Professor, DTU for his technical suggestions.

**Kamini Sharma**

# CONTENTS

## LIST OF TABLES

## LIST OF FIGURES

## LIST OF ABBREVIATIONS

| | |
|---|---|
| LULC | Land Use Land Cover |
| PRISMA | PRecursore IperSpettrale della Missione Applicativa |
| CNMF | Coupled Nonnegative Matrix Factorization |
| SVM | Support Vector Machine |
| ISA | Impervious Surface Area |
| UGS | Urban Green Space |
| UGSA | Urban Green Space Area |
| NDBI | Normalized Difference Built-up Index |
| CNN | Convolutional Neural Networks |
| ENMAP | Environmental Mapping and Analysis Program |
| GS | Gram-Schmidt |
| PCA | Principal Component Analysis |
| PAN | Panchromatic |
| MRA | Multiresolution analysis |
| HSI | Hyperspectral Image |
| NIR | Near Infrared |
| VNIR | Visible Near Infrared |
| SWIR | Short-wave Infrared |
| UHI | Urban Heat Island |
| LST | Land Surface Temperature |
| ML | Maximum Likelihood |
| OBIA | Object-Based Image Analysis |
| NDVI | Normalized Difference Vegetation Index |
| EVI | Enhanced Vegetation Index |
| SAVI | Soil-Adjusted Vegetation Index |

| | |
|---|---|
| RF | Random Forest |
| IHS | Intensity-Hue-Saturation |
| NMF | Non-Negative Matrix Factorization |
| NCT | National Capital Territory |
| TCC | True Color Composite |
| PHSI | PRISMA hyperspectral imagery |
| TIFF | Tagged Image File Format |
| MNF | Minimum Noise Fraction |
| RBF | Radial Basis Function |

# CHAPTER 1

# INTRODUCTION

## 1.1 MOTIVATION

Hyperspectral remote sensing is a recent and significant achievement in the remote sensing community. It offers valuable spectral information per pixel and overcomes the challenges of mixed pixels and spectral similarity often encountered in multispectral data [1]. With hundreds of contiguous bands, hyperspectral data provides rich information for discrimination studies and accurate classification mapping. High spatial spectral-resolution remote sensing data has the potential to produce detailed maps of urban materials and their condition, which is important since over two-thirds of the world's population now lives in urban areas. [2] Urbanization can result in social and environmental challenges such as loss of vegetation cover, poor air and water quality, microclimate changes, and thus deterioration of public health [3]. For urban planners and decision-makers, the built-up urban area is an important reference for assessing the city's level of development and planning future changes. Urban analysis is difficult due to the complexity and diversity of urban surfaces over a small area. Therefore, regular monitoring and updating of maps is essential in urban areas, where objects are mobile and infrastructure, vegetation, and construction are constantly changing [3,4]

## 1.2 BACKGROUND TO REMOTE SENSING

By monitoring the radiation reflected or emitted by the objects, remote sensing collects information about those objects. Image data is typically used to represent this information which is collected from far away [5]. For finding items above and below the Earth's surface, remote sensing has the potential to be an efficient technique. It typically entails the use of sensors mounted on aerial or space-based platforms to gather data about the Earth's surface and atmosphere utilising electromagnetic radiation as the data carrier. There are two different kinds of sensors: passive ones that pick up ambient radiation and active ones that emit their own electromagnetic radiation. There are two

subcategories of remote sensing: optical and microwave [6]. Through the use of sensors, optical remote sensing creates images that resemble photographs taken by a camera/sensor in space by detecting sun light at various wavelength areas [7]. Additionally, there are four different types of resolution: spatial, spectral, temporal, and radiometric. These categories describe, in turn, the size of each pixel within an image, a sensor's capacity to define precise wavelength intervals, the amount of time it takes a satellite to return to an observation area, and the quantity of bits used to represent the energy or information contained in each pixel [8].

## 1.3 URBAN FEATURE EXTRACTION

The technique of locating and extracting significant data or characteristics from satellite imagery of urban areas is known as "Urban feature extraction" [9].

Roads, buildings, vegetation, bodies of water, and other man-made or natural objects are examples of these features. Various algorithms and approaches are used to analyse the satellite image data and extract pertinent features throughout the feature extraction process. Image segmentation, edge detection, and object recognition are a few typical methods used in satellite image feature extraction [10].

The process of picture segmentation involves dividing up the satellite image into more manageable, smaller regions or portions. This may make it simpler to recognise and extract particular characteristics from the image, such as vegetation or buildings.

Edge detection is a method for locating the borders or edges of objects in a picture. For locating things like highways, rivers, or other linear characteristics, this can be helpful.

Utilising machine learning methods, object recognition identifies specific objects in the satellite image. This can be especially helpful for distinguishing objects like buildings, which may have recognisable shapes or patterns that a computer can recognise.

These features can be utilised for a variety of purposes, such as urban planning, environmental monitoring, and disaster response, once they have been recognised and retrieved from the satellite image. For instance, the extraction of features from satellite images can be used to follow the spread of wildfires or other natural disasters, observe changes in land use patterns over time, or pinpoint regions that may be vulnerable to flooding or other dangers [11]. Overall, the ability to extract features from satellite

images is a strong tool that can offer insightful data and information for a variety of applications and sectors.

## 1.4 ISSUES WITH URBAN FEATURE EXTRACTION

Urban feature extraction is a useful tool for managing urban environments, but there are a few problems that might occur throughout the process. These problems are as follows [12]:

Urban environments can be quite complex, with a variety of features and items that must be recognised and retrieved from satellite photos. The feature extraction procedure may become more difficult and time-consuming as a result.

Scale: Because urban areas can be very big, it may be necessary to process a significant amount of satellite images in order to extract features from the entire region. This could be quite resource-intensive and computationally demanding.

Data quality: The accuracy of feature extraction results might be affected by the quality of satellite imagery, which can vary. The quality of the data may be impacted by factors such as cloud cover, atmospheric conditions, and sensor calibration.

Accuracy of classification: Depending on the chosen classification scheme, feature extraction methods' accuracy can change. The overall accuracy of the results may be impacted by the use of various classification systems that are better suited to various kinds of characteristics or objects.

Even with sophisticated feature extraction techniques, deciphering the generated features might be difficult. For instance, it may be necessary to have additional information and skills in order to discern between various building or land use types beyond what can be learned from satellite imaging alone.

Overall, even though urban feature extraction can offer insightful data and knowledge for a variety of applications, it is crucial to be aware of these problems and take action to resolve them in order to assure accurate and trustworthy findings [10,11].

## 1.5 IMAGE FUSION

To generate one image having more information than any of the individual images, two or more satellite images of the same geographic area captured by different sensors or modalities are combined in a process known as Satellite Image fusion [16]. Enhancing the quality of the images and offering a more thorough and accurate depiction of the geographic area are the two main objectives of satellite image fusion.
Many methods, including pixel-based, feature-based, and decision-based fusion, can be used to combine satellite images. In pixel-based fusion, the different images' pixel values are combined to produce a single fused image. In feature-based fusion, features are extracted from the constituent images before they are combined to form a fused image. Making decisions based on the data in each separate image, followed by integrating the outcomes to produce a fused image, is known as decision-based fusion.[13]

The importance of satellite image fusion can be attributed to a number of factors. One of the key benefits is that it can improve the image quality and resolution. Satellite image fusion can offer a more thorough and accurate depiction of the geographic area by integrating images from several sensors or modalities. This can aid with feature extraction and more precise image classification processes. [14,15]

## 1.6 LITERATURE REVIEW

### 1.6.1 Urban feature Extraction – Impervious Surface areas

A novel method for identifying road networks in high resolution satellite imagery was proposed by **Singh and Garg (2013)** [17]. There are three main steps in the suggested procedure. In order to separate highways from the cropped image, they first perform adaptive global thresholding. Then, using morphological techniques, they remove brief non-road parts to extract the road network. The recovered road network and the region with similar pixel intensity values are then used to construct a spatial road matrix. The locations of potential non-road portions are shown by the road matrix. After extracting only, the road networks from the road matrix using a road tracking technique, certain additional morphological procedures are performed. The correctness and completeness criteria were employed to assess how accurate the road network

extraction is, and the results were 96.52 and 95.32, respectively. This showed a high level of accuracy in the road network extraction.

An overview of mapping approaches for ISA mapping was presented by **Lu et al. (2014)** [18]. They talked about how scale affects remote sensing data and associated algorithms and emphasised the need for innovative approaches to boost ISA mapping and estimate performance. When choosing remote sensing data and associated factors and creating an ideal technique, scale is a crucial factor. Very high spatial resolution photos are necessary for ISA mapping at the local level, and segmenting or using textures to represent spatial information is a good technique to enhance ISA mapping performance. For ISA mapping of specific cities, many medium spatial resolution images were used, and merging multi-resolution/sensor data has proven useful in enhancing ISA spatial patterns. The ISA area estimates can be significantly improved by SMA-based techniques. The distinction between ISA and other land coverings must be strengthened using the appropriate data fusion techniques. It is also beneficial to post-process data utilising auxiliary information like population density and land surface temperature. For study on population, economic, and environmental issues on a national and international scale, timely updating of ISA data sets is required.

**Aishwarya et al.** (2017) [19] suggested a method for extracting water, land, and built-up urban characteristics from Enhanced Thematic Mapper Plus (ETM+) (Landsat 7) imagery. The three indices used in the study were the Normalised Difference Water Index (NDWI), the Normalised Difference Vegetation Index (NDVI), and the Normalised Difference Built-up Index (NDBI), each of which represents one of the three main elements of Earth: an open water body, vegetation, or built-up land. From the seven original Landsat 7 image bands, these indices were utilised to produce three thematically focused bands, which were then combined to produce a new image. The accuracy ranged from 91.5 to 98.5 percent as a result of reducing data correlation and redundancy between the original multispectral bands.

In order to make the process of extracting impervious surfaces easier while also disguising permeable surfaces like bare soil, **Fang and colleagues (2019)** [20] proposed a ratio-based impervious surface index (RISI) that makes use of Landsat 8 multispectral remote sensing images. The results were compared with those obtained from five other

methods for extracting the distribution of impervious surfaces, including the Normalised Difference Built-Up Index (NDBI), the Built-Up Index (IBI), the Normalised Difference Impervious Surface Index (NDISI), the Normalised Difference Infrared Index (NDII), and the Composite Burn Index (CBI). The researchers tested this index on three representative images of urban areas in China during both the winter and summer. The results suggested that RISI demonstrated good performance in differentiating impermeable surfaces from other ground objects, particularly bare soil, and showed a precision rate of 95%, 91%, and 93%, respectively.

A method for extracting built-up area features from remote sensing images using the bat algorithm and normalised chromatic aberration was proposed by **Xun et al. (2019)** [21]. Prior to highlighting the colour features, the strategy first improved the contrast of remote sensing images. The features were then binarized after the colour of each feature was retrieved using normalised chromatic aberration. In comparison to CNN, the suggested method used less training sets and outperformed traditional image-enhancing techniques. The ROI was extracted using the normalised method following the optimisation of the bat algorithm, yielding a high extraction rate of up to 96%.

Using information from the Sentinel-2A and Landsat-8 satellites, **Deliry et al. (2021)** [22] evaluated and contrasted the efficacy of five classification algorithms in identifying urban impervious surfaces. The algorithms put to the test included the band ratioing normalised difference built-up index (NDBI), normalised difference impervious index (NDII), supervised object-based nearest neighbour (NN) classifier, supervised pixel-based maximum likelihood classifier (MLC), and supervised pixel-based spectral angle mapper (SAM). The outcomes demonstrated that, among the investigated methods, the supervised object-based NN strategy created the most precise and consistent map. For Sentinel-2 and Landsat-8 pictures, the algorithm achieved classification accuracy of 90.91% and 88.64%, as well as a Kappa coefficient of 0.82 and 0.77, respectively. In comparison to the object-based NN approach, the supervised pixel-based MLC method created less homogeneous maps but still delivered satisfactory results. On the other hand, the semi-automatic NDBI and NDII methods as well as the SAM algorithm were unable to produce classification accuracy that was satisfactory.

For efficient feature extraction in complicated metropolitan environments using hyperspectral pictures impacted by cloud shadows, **Ma et al. (2023)** [23] suggested a unique 3D-1D-CNN model. The hyperspectral data was initially used to extract the spectral composition parameters, vegetation index, and texture features. Following the fusion and segmentation of these parameters into several patches, a 3D-CNN classifier was employed to extract features from complicated urban landscapes. For comparison reasons, a number of classifiers, including SVM, RF, 1D-CNN, 3D-CNN, and 3D-2D-CNN, were also used. In order to assess the accuracy, a confusion matrix and Kappa coefficient were calculated. The accuracy of the proposed 3D-1D-CNN model was 96.32% overall, outperforming SVM, RF, 1D-CNN, and 3D-CNN classifiers by 23.96%, 11.02%, 5.22%, and 0.42%, respectively. According to these findings, the 3D-1D-CNN model successfully extracts spatial-spectral information from hyperspectral data, particularly in cloud shadow areas where spectral information is lacking, such grass and motorways. In the future, the proposed concept might potentially be applied to the extraction of urban green areas.

### 1.6.2 Urban feature Extraction – Urban Green Space

The effectiveness of land cover classification and data from the Normalized Difference Vegetation Index (NDVI) were compared in a study done by **Li and colleagues in 2015** [24] to determine the economic worth of green urban areas in California. They discovered that high-resolution categorized land cover images are preferred over NDVI in hedonic models meant to evaluate the economic advantages of urban greening programmes, despite their higher cost, even if NDVI data with intermediate resolution may be sufficient for evaluating economic gains.

**Aram et al.'s** [25] assessment of previous studies that looked at the cooling effects of urban green areas was published in **2019**. Based on the methodologies utilized for evaluation, the study was split into three categories. The first category mostly used remote sensing and satellite maps to evaluate urban green spaces in one or more cities. The second group used on-the-ground observations to investigate city parks or several urban parks. The third category entailed simulating a part of urban land under various placement scenarios for green space. According to the analysis, huge urban parks with

an area larger than 10 hectares were areas where the greatest cooling impact distance and intensity were found to be present.

Urban green spaces (UGS) were mapped in 1039 mid- and large-sized cities worldwide in 2015 using dense remote sensing data and the Google Earth Engine (GEE) platform. **Hung et al. (2021)** [26] also evaluated the spatial distribution and accessibility of UGS within the cities. To distinguish UGS from other vegetation, they combined the greenest pixel compositing method and the percentile-based image compositing method, which produced higher accuracy (89.26%). In contrast to cities in low- to lower-middle-income countries, they discovered that high-income cities had higher UGSC and UGSA values.

### 1.6.3 Urban feature Extraction – LULC

In an experiment, **Jozdani and coworkers (2019)** [27] compared a variety of deep neural network architectures (including regular deep multilayer perceptron, regular autoencoder, sparse autoencoder, variational autoencoder, and convolutional neural networks), ensemble algorithms (such as Random Forests, Bagging Trees, Gradient Boosting Trees, and Extreme Gradient Boosting), and Support Vector Machines (SVM) to assess their efficacy in urban mapping using GEOBIA. Two remote sensing images with resolutions of 30 cm and 50 cm were used to test the classifiers. They came at three key conclusions from their experiment: First, the most effective classifier was the MLP model. Second, utilizing autoencoders for unsupervised pretraining did not enhance classification outcomes. Thirdly, it was demonstrated that these cutting-edge machine learning classifiers are adaptable enough to handle the mapping of complicated landscapes by comparing the tiny changes in classification accuracy between MLP and other models like SVM, GB, and XGB. They discovered that combining CNN and GEOBIA did not yield in results that were more accurate than those produced by the other classifiers they had employed.

By analyzing four key research studies, **Moharram and Sundaram (2023)** [28] completed a thorough and systematic study of land use and land cover (LULC) categorization using hyperspectral images. They first spoke about the essential elements of hyperspectral imaging, various hyperspectral imaging modes, data gathering

techniques, and important distinctions between hyperspectral and multispectral pictures. Second, they discussed a number of common deep learning techniques, including Convolutional Neural Network (CNN), Stacked Autoencoder (SAE), Deep Belief Network (DBN), Recurrent Neural Network (RNN), and Generative Adversarial Network (GAN). They also examined the role of machine learning in LULC classification. Thirdly, they examined common benchmark hyperspectral datasets and the standards for measuring the effectiveness of LULC classification techniques.

In their **2011** study, **Gamba and colleagues** [29] attempted to simulate the urban environment at a low spatial resolution, comparable to the new hyperspectral sensor-ENMAP. The study's goal was to learn more about the new sensors' capabilities in a challenging environment such as in very mixed images, Low spatial resolution is a challenge for studying urban landscapes, according to experiments done on real datasets. The findings showed that defining urban regions is a very difficult assignment, in a scenario with a low spatial resolution.

**Dobhal's** master's thesis from **2008** [30] focused on classifying and extracting features from Hyperion data. Gram-Schmidt, Principal Component, and Colour Normalized Transform were three fusion techniques that were utilized in the study to combine high-resolution IKONOS data with Hyperion data. For spectral assessment, which involved examining the spectral profiles of various land use and land cover (LULC) classes, the fused products were compared to Hyperion data. The different LULC classes in the original IKONOS and the three fused products were manually delineated in order to perform the spatial evaluation of the three merged products. The spectral evaluation's findings demonstrated that the CN spectral sharpening approach retained the spectral characteristics of the fused product more effectively. The three fused products' spatial quality significantly improved when compared to the Hyperion data, but not when compared to the IKONOS data, according to the qualitative evaluation of the different LULC classes. The separability research also revealed that the fusion improved some classes' separability, leading to greater classification accuracy. The highest classification accuracy that could be achieved was 80%.

### 1.6.4 Image Fusion Techniques

In research done by **Loncan et al. (2015)** [31], they evaluated several pan-sharpening methods for hyperspectral data with cutting-edge multispectral pan-sharpening approaches that were modified for hyperspectral data. Eleven distinct approaches from diverse classifications, including component substitution, multiresolution analysis, hybrid, Bayesian, and matrix factorization, were assessed for their efficacy and resilience. Utilizing well-known performance measures, the approaches were applied to three separate datasets that represented various circumstances. They also developed a MATLAB toolbox that was made public and contains all the pan-sharpening methods. Based on their effectiveness, the study's findings divided the approaches into four categories. The first category included techniques like GFPCA and CS-based algorithms (GS and PCA) that produced subpar fusion outcomes. The second set of approaches (MRA methods, GSA, and Bayesian naive) are appropriate for fusing large-scale images, which is frequently the case for spaceborne hyperspectral imaging missions. These methods have strong fusion performances and cheap processing costs. Methods with slightly better fusion outcomes but higher computational costs (HySure and Bayesian Sparse) made up the fourth group, whereas those with slightly better fusion results but lower computational costs (CNMF) made up the third group.

Through pan-sharpening and fusion strategies, **Mookambiga and Gomathi (2016)** [32] reviewed the different methods for improving the resolution of hyperspectral images (HSI). They divided the methods into two groups: hyperspectral image fusion with multispectral pictures and hyperspectral pan-sharpening (using PAN images). Most methods employed for multispectral pan-sharpening, they observed, could be adjusted for use in hyperspectral pan-sharpening. The study presents matrix factorization and Bayesian approaches created particularly for HS pan-sharpening and offers a review of traditional methods for HSI pan-sharpening, such as CS and MRA. The study also covered recommended performance evaluation metrics and datasets that were made accessible for the fusion process.

"Hyper-sharpening" is a brand-new idea in remote sensing image fusion that **Selva et al. (2015)** [33] aimed to introduce. The old method of pan-sharpening, according to the authors, is constrained and insufficient, especially when new

instruments are created. In situations where multispectral or hyperspectral data is utilized to extract spatial information, the phrase "hyperspectral (HS) pan-sharpening" exists; however, it is not clearly defined. The authors suggested a hyper-sharpening framework and two hyper-sharpening techniques to solve this. Data from the improved SIM-GA imager, which comprises a panchromatic camera and two spectrometers in the VNIR and SWIR spectral regions, was used for the studies. Hyper-sharpening was used to fuse SWIR data to VNIR resolution by accounting for the various resolution variables across the data sets.

A novel hyper-sharpening approach based on spectral modulation was presented by **Lu et al. (2019)** [34] with the goal of better preserving spectral information while merging MS data from a separate sensor with HS data. The framework tries to provide an adjusted MS picture that would have been taken under the identical imaging circumstances as the associated HS sensor. The authors introduced the high-pass details injection model and the band-dependent spatial-detail model, two methods derived from MS pan-sharpening. The suggested framework was put to the test on three HS and MS datasets gathered from various platforms, and the findings revealed that it was superior to existing hyper-sharpening strategies in terms of maintaining spectral integrity and increasing spatial details. In particular, when there are notable changes in acquisition dates and circumstances, the research emphasizes the significance of modulation processing for genuine HS and MS data.

To create fused data with high spectral and spatial resolutions, **Yokoya and colleagues (2011**) [35] suggested a method for combining low-spatial-resolution hyperspectral and high-spatial-resolution multispectral data. Their technique, known as Coupled Nonnegative Matrix Factorization (CNMF), alternatively unmixed the hyperspectral and multispectral data into endmember and abundance matrices using a linear spectral mixing model. Each NMF unmixing procedure's initialization matrix included sensor observation models that connected the two sets of data. These two matrices might be used to provide fused data with high spectral and spatial resolutions. The CNMF technique was proved to be physically simple and simple to use, and by establishing a high number of endmembers, it could handle spectrally shifting scenes. The CNMF outperformed the MAP/SMM algorithm, one of the most cutting-edge algorithms currently in use, according to simulations. The CNMF approach's high-

quality fused data might make it easier to correctly identify and categorize objects seen at a high spatial resolution.

## 1.7 RESEARCH GAPS

In reviewed literature, the following research gaps were observed:

1. Data used for extracting urban features was usually multispectral.
2. In case where Hyperspectral data is used, no recent data is used. Recent data can be better utilized for latest monitoring urban areas.
3. Fewer studies were done in India and almost no study was found to be conducted in Indian national capital Delhi using hyperspectral data for mapping or extraction of urban features.
4. Image Fusion or Hyper-sharpening techniques for improving the classification and feature extraction results over city Delhi was also not explored.

## 1.8 RESEARCH OBJECTIVES

**Objective 1** – Hyper-Sharpening of satellite data over city Delhi.

**Objective 2** – Extraction of Urban Features using the Hyper-Sharped data.

## 1.9 ORGANISATION OF THESIS

This thesis comprises five chapters. The first chapter describes the motivation for the study and introduces remote sensing, urban feature extraction, and image fusion. The chapter also highlights the challenges associated with urban feature extraction. It includes a literature review, identifies research gaps, and lists research objectives. The second chapter briefs about different urban features, their extraction methods and image sharpening techniques. The third chapter presents the study area, explains the resources used, outlines the methods followed. The fourth chapter reports the observations, obtained results and comments related to them. Finally, the fifth chapter provides concluding remarks on the study's findings and discusses this research’s contribution future directions.

## 2.1 IMPERVIOUS SURFACE AREA

Impervious surface area (ISA) refers to the surfaces that do not allow the penetration of water into the soil, such as roofs, roads, pavements, and other similar surfaces. The increase in impervious surfaces has been identified one of the primary causes of environmental degradation in urban areas, as it alters the hydrological cycle and increases the risk of urban flooding, water pollution, and degradation of aquatic ecosystems. [17,20,22]

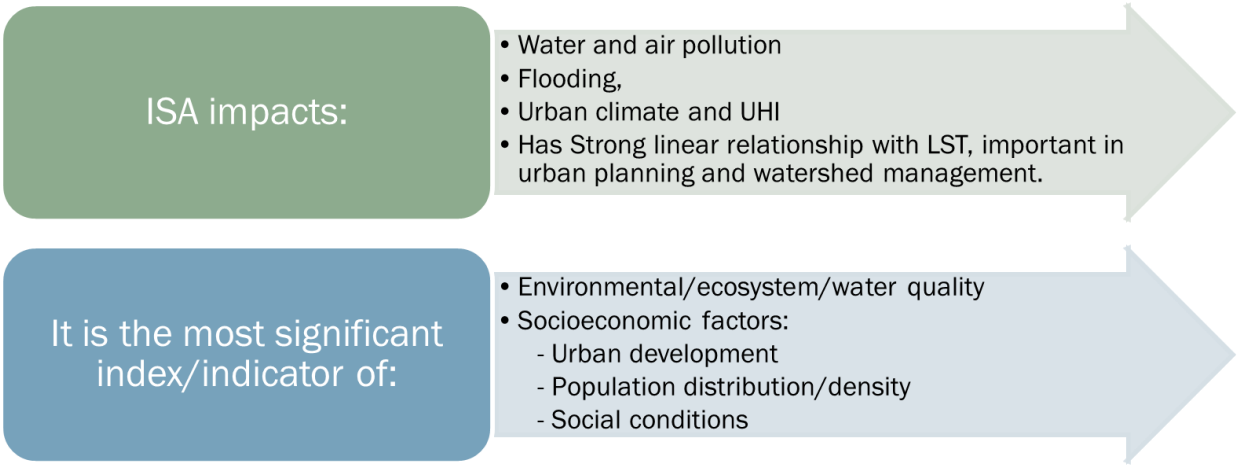


**Figure 2.1** Importance of Impervious Surface area (ISA) [17,18,20,22]

Remote sensing, particularly satellite imagery, is widely used to extract ISA as it can provide a synoptic view of the Earth's surface, allowing for large-scale mapping and analysis. There are several methods [36,40,41] used to extract ISA from satellite images, which are classified into two categories: Spectral and Spatial methods.

1. **Spectral Methods**

   Spectral techniques rely on impermeable surfaces' distinctive spectral signature, which may be separated from other forms of land cover. There are two popular spectral techniques:

- **Spectral Indices**

  The reflectance values of several satellite image bands are combined mathematically to create spectral indices, which emphasize particular land cover types. The Normalized Difference Built-up Index (NDBI) is the spectral index that is most frequently utilized for ISA extraction. NDBI is determined by:

$$NDBI = \frac{(\text{SWIR} - \text{NIR})}{(\text{SWIR} + \text{NIR})}$$

  where NIR stands for near-infrared and SWIR for shortwave infrared. Impervious surfaces are indicated by NDBI values near to 1, whereas vegetated regions are indicated by values close to 0.

- **Classification Methods**

  Classification methods use statistical algorithms to classify the diverse land cover types present in the satellite image. The most commonly used classification method for ISA extraction is the supervised classification method, where the user selects training samples of different land cover types, which are used to train the algorithm to classify the remaining pixels. The commonly used classifiers for ISA extraction are Support Vector Machines (SVM) and Maximum Likelihood (ML) [37,38].

**2. Spatial Methods**

Spatial methods depend on the spatial properties of impervious surfaces, such as their shape, size, and texture. There are two commonly used spatial methods:

- **Object-Based Image Analysis (OBIA)**

  OBIA is a process where the satellite image is segmented into objects created on their spectral, textural, and spatial properties. The objects are then classified based on their shape, size, and texture to distinguish impervious surfaces from other land cover types.[46]

- **Fractal Dimension**

  Fractal dimension measures the complexity of the surface by analysing the spatial dispersal of pixels in the imagery. The fractal dimension of impervious

surfaces is higher than other land cover types due to their complex shape and texture. The commonly used method for fractal dimension analysis is the Box Counting method. [42,43,44,45]

The accuracy of ISA extraction depends on several factors, including the size of the pixel in the satellite image, the accuracy of ground truth data, and the appropriateness of the method used. The accuracy of spectral methods is limited by the spectral resolution of the satellite image, while spatial methods can be affected by the segmentation and classification algorithms used.

Thus, Remote sensing, particularly satellite imagery, provides a valuable tool for ISA extraction, allowing for large-scale mapping and analysis. The choice of method for ISA extraction depends on the specific characteristics of the satellite image and the research objectives. Spectral methods are suitable for large-scale mapping, while spatial methods are suitable for detailed analysis of individual objects. The accurateness of ISA extraction can be enhanced by merging multiple methods and ground truth data.

## 2.2 URBAN GREEN SPACE

The UGS or Urban Green Spaces are zones in cities that are covered with vegetation, including street trees, parks, green roofs, gardens and other types of vegetation. UGS offers various environmental, social, and economic benefits to urban residents. These advantages include bettering the quality of the air and water, reducing the impact of the urban heat island, offering recreational possibilities, enhancing mental health and well-being, and increasing property values. With the increasing demand for UGS, it has become essential to monitor and assess the distribution and extent of green spaces in urban areas. Satellite imagery provides an efficient and cost-effective way to map and monitor UGS. Several techniques have been created recently to extract UGS from satellite images. One of the most commonly used methods for extracting UGS is object-based image analysis (OBIA). [47]

OBIA is a method that involves dividing an image into smaller segments or objects based on their spatial, spectral, and textual attributes. Once these objects are identified, they are classified into different land cover types, including UGS. The OBIA

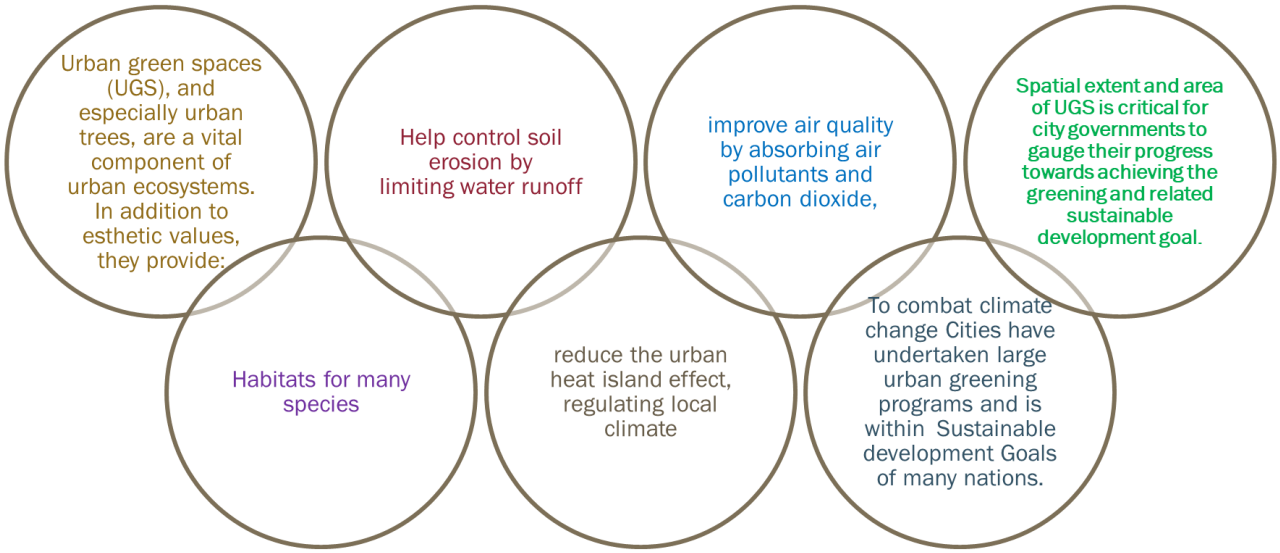


**Figure 2.2** Importance of Urban Green Space (UGS).

method requires the selection of appropriate segmentation parameters, such as object size, shape, and texture, which affect the accuracy of the results. To improve the accuracy of UGS extraction, various features, such as texture, shape, size, and vegetation indices, can be used as input parameters in the classification algorithm.[48]

The Normalized Difference Vegetation Index (NDVI) is a different technique for UGS extraction. The difference between the reflectance of near-infrared and red light bands is measured by the vegetation index known as the NDVI. The NDVI values range from -1 to 1, with values closer to 1 denoting a higher vegetation density. The NDVI method has been used to map UGS by setting a threshold NDVI value above which the pixels are classified as UGS.[49]

However, the NDVI method has limitations, such as its inability to differentiate between different types of vegetation and its sensitivity to atmospheric effects, which can affect the accuracy of the results. To overcome these limitations, various modifications of the NDVI, like the Soil-Adjusted Vegetation Index (SAVI) and Enhanced Vegetation Index (EVI) have been developed.[50]

Another approach for UGS extraction is machine learning algorithms. UGS has been categorized as a land cover type using machine learning methods like Random Forest and Support Vector Machines. Machine learning algorithms require a training dataset with labelled UGS and non-UGS pixels, which are used to develop a classification model. The classification model is then applied to the entire image to map the UGS. Machine learning algorithms have been shown to provide accurate results for UGS extraction, but they require a large training dataset and may not perform well when applied to different geographic locations or different seasons due to variations in the spectral properties of vegetation.

In addition to the above methods, deep learning algorithms, such as Convolutional Neural Networks (CNN), have recently been used for UGS extraction. CNNs are a particular kind of machine learning algorithm that can automatically learn to recognize characteristics from visual data. CNNs have shown promising results for UGS extraction, but they require a large training dataset and significant computational resources. [47, 51]

Thus, in the view of UGS importance to urban residents, and its extent and distribution need to be monitored and assessed regularly. Using satellite imaging, it is possible to monitor and map UGS effectively and economically. The level of accuracy needed, the kind of vegetation, the size of the region, and the available computational resources are only a few of the variables that influence the choice of an acceptable UGS extraction technique.

## 2.3 LAND COVER AND LAND USE

The terms "land cover and land use" (LCLU) relate to both the physical covering of the land surface and the method in which it is used. The term "land use" refers to the various human activities that are carried out on the land, including forestry, mining, urbanization, agriculture, and recreation.[52] The physical characteristics of the land surface, such as forests, marshes, grasslands, aquatic bodies, and urban areas, are referred to as land cover. Changes in land use and land cover have a substantial impact on climate change, the preservation of biodiversity, the management of water resources, and sustainable development.[53]

Geographic information systems (GIS) and remote sensing both depend on the production of LULC maps. LULC maps offer useful data for planning land use, managing natural resources, and keeping an eye on the environment. Depending on the goals, spatial resolution, spectral and temporal properties of the satellite pictures, and the needed level of accuracy, there are many techniques for producing LULC maps.[54]

A popular technique for producing LULC maps is supervised classification. For each land cover class in supervised classification, a collection of representative training samples is chosen. From the satellite pictures, these training samples are utilized to extract spectral signatures or features that are then used to categorize the pixels into various land cover classes. The quality and representativeness of the training samples, the land cover classes' spectral separability, and the classification algorithm's application all affect how accurate the classification is. Maximum Likelihood, Support Vector Machine, Decision Tree, and Artificial Neural Networks are a few of the frequently used supervised classification techniques.[54]

Another method for creating LULC maps is unsupervised classification. In unsupervised classification, the satellite images are classified into clusters or groups based on their spectral similarity. The number and nature of the clusters depend on the clustering algorithm used and the similarity measures employed. The clusters are recognized, and then based on their spectral properties and visual interpretation, they are classified into several land cover groups. When the quantity and makeup of the land cover classes are unknown or when the spectral separability of the classes is poor, unsupervised classification might be helpful. However, unsupervised classification may lead to misclassification and confusion between similar land cover classes.[54]

There are many algorithms that are used in supervised or unsupervised method of classification.: [57,58]

1. **Maximum Likelihood Classification**: A popular approach for LULC classification is Maximum Likelihood Classification (MLC). The method determines the chance of a pixel belonging to each class based on the presumption that every pixel in an image belongs to a certain class. The pixel is given the class with the highest probability.

2. **Support Vector Machine**: A supervised learning method used for classification problems is called the Support Vector Machine (SVM). It operates by identifying the class border that optimizes the margin between them. Both binary and multiclass classification may be done using SVM.

3. **Random Forest:** Multiple decision trees are used in the Random Forest (RF) ensemble learning process to build a classification model. Each decision tree is made by randomly choosing a subset of characteristics and a subset of data. The majority vote of all the decision trees is used to determine the final categorization.

4. **Artificial Neural Networks:** Artificial Neural Networks (ANNs) are a group of methods that are designed to mimic the way the human brain works. They are used for classification tasks and can be trained using supervised or unsupervised learning methods.

5. **Decision Trees**: A straightforward and efficient approach for LULC classification is called a decision tree (DT). Recursively dividing the data into subgroups according to the values of the characteristics, they then give each subset a class.

6. **Spectral Angle Mapper**: The spectral signature of each pixel in an image is compared to a collection of reference spectra using the spectral matching method known as Spectral Angle Mapper (SAM). The class whose spectral angle is most similar to the pixel's own spectral signature is given to it.

**Object-Based Image Analysis**: Object-based image analysis (OBIA) is also a method for creating LULC maps. OBIA involves segmenting the satellite images into meaningful and homogeneous objects based on their spectral, spatial, and textual properties. The objects are then categorised into different land cover classes based on their physical and environmental characteristics, such as shape, size, texture, context, and location. OBIA is useful when the spatial resolution of the satellite images is high and when the land cover classes are complex and heterogeneous, such as urban areas, agricultural fields, and forests. OBIA has been successfully applied in various LULC mapping projects, such as land-use planning, forest inventory, and urban growth analysis.

The selection of algorithm will rely on the details of the data and the classification job at hand because each of these algorithms has strengths and drawbacks of its own. In practice, a combination of these algorithms may be used to create accurate and reliable LULC maps.[54]

## 2.4 PANSHARPENING, IMAGE FUSION AND HYPER-SHARPENING

Two remote sensing techniques are used to increase the information content of satellite images: pan-sharpening and satellite image fusion.

**Pan-sharpening** is a method of fusing a high-resolution (panchromatic) grayscale image with a less-resolution multispectral image to create a higher-resolution, multispectral image. The goal of pan-sharpening is to increase the spatial resolution of the multispectral data, while retaining its spectral information. This technique is particularly useful in various areas land cover classification, where high-spatial resolution is important for identifying small features, such as buildings or trees, while spectral information is necessary for distinguishing between different land cover types.[64]

**Satellite image fusion**, on the other hand, involves combining two or more satellite images (can be radar and multispectral) of the same location, acquired at different times or using different sensors, to create a single composite image. The aim of image fusion is to create a more complete image with a higher level of detail than any of the individual images. This technique is particularly useful for monitoring land cover changes over time or detecting changes in the environment, such as flooding or forest fires. [60, 61]

**Hyper-sharpening** is a technique used to decrease the size of the pixel of hyperspectral images by combining them with high-resolution panchromatic images.[72] The aim is to produce an imagery that combines the high spectral resolution part of hyperspectral image with the high spatial resolution part of panchromatic image. The key benefit of hyperspectral imagery is its capability to capture and distinguish spectral information for each pixel. However, hyperspectral imagery o spatial resolution is generally lower than that of panchromatic images. Hyper-sharpening overcomes this limitation by integrating the spectral and spatial information from both sources to

produce an image that has both high spectral and spatial resolution [71]. There are several techniques for hyper-sharpening [62, 65, 66, 67, 68, 69, 70]. Here are a few:

**Pixel Swapping**: In this method, the relevant pixels in the lower resolution hyperspectral picture are swapped out for those in the high-resolution panchromatic image. While the spatial information is enhanced by adding the panchromatic image, the spectral information from the hyperspectral image is kept. This technique's drawback is that it could lead to spectrum distortion and noise amplification.

**Gram-Schmidt sharpening** combines hyperspectral data with panchromatic imagery to enhance spatial resolution. It involves pre-processing, spectral adjustment, Gram-Schmidt transformation to decorrelate hyperspectral bands, fusion with panchromatic band, and an inverse transformation. By leveraging panchromatic data, it improves spatial details in hyperspectral data, resulting in a fused image that retains both spectral and spatial information. Its drawback is that it works well only with hyperspectral data spectral range overlapping pan's spectral range, for other ranges of hyperspectral data, spectral information is deteriorated.

**Principal Component Analysis (PCA)**: PCA is a method used for reducing dimensionality in hyperspectral imagery. It involves transforming the hyperspectral image into a group of uncorrelated components. In hyper-sharpening, PCA uses panchromatic image to extract the spatial information and then inject it into the hyperspectral image. The algorithm operates under the assumption that the spectral bands with less spatial resolution are related to the panchromatic band with higher spatial resolution.

**Intensity-Hue-Saturation (IHS) Transform**: Another method for combining the spatial and spectral data from hyperspectral and panchromatic pictures is the IHS transform. The panchromatic picture is combined with the intensity, hue, and saturation components that were previously extracted from the hyperspectral image. While the hue and saturation components represent the spectral information, the intensity component represents the spatial information.

**High-Pass Filtering**: High-pass filtering is a technique used to remove the high-frequency components from an image. In hyper-sharpening, the high-pass filter is used over the panchromatic image to extract the high-frequency details, which are then merged with the corresponding pixels in the hyperspectral image.

**Wavelet-Based Methods:** Wavelet-based methods involve decomposing the hyperspectral and panchromatic images into wavelet coefficients. Extracted from the panchromatic picture, the high-frequency components are combined with the corresponding pixels in the hyperspectral image.

**Matrix Factorization**: NMF unmixing is used alternatively to low-spatial-resolution hyperspectral and high-spatial-resolution multispectral data in Coupled Nonnegative Matrix Factorization (CNMF), a method for collecting data with high spatial and spectral resolutions. As a consequence, high-spatial-resolution abundance matrices and hyperspectral endmembers are obtained. These two matrices can be used to provide data with great spectral and spatial resolutions.

**Bayesian methods** for hyperspectral sharpening use Bayesian inference principles to fuse low-resolution hyperspectral data with higher-resolution spatial information. They involve constructing a statistical model, specifying priors (to represent prior knowledge about the scene), estimating likelihood, performing Bayesian inference, and fusing the spatial image with high-resolution hyperspectral image. These methods provide a probabilistic framework for incorporating prior knowledge and uncertainties, resulting in sharper and more accurate images. However, they require computational resources and careful parameter tuning.

Hyper-sharpening, then, is a method that combines high-resolution panchromatic photos with hyperspectral images to enhance their spatial resolution. The particulars of the images being fused, as well as the required level of accuracy and processing efficiency, all influence the method that is selected.

# CHAPTER 3

# DATA AND METHODOLOGY

## 3.1 AREA OF STUDY

This research is located in Delhi, India (Fig. 3.1). Delhi, the nation's capital, is both a city and a union territory, and its official name is the National Capital Territory of Delhi (NCT). The NCT has a total size of 1,484 square kilometres. In 2011, the population of Delhi's core exceeded 11 million, making it India's second-largest metropolis after Mumbai. About 16.8 million people made up the NCT's whole population.

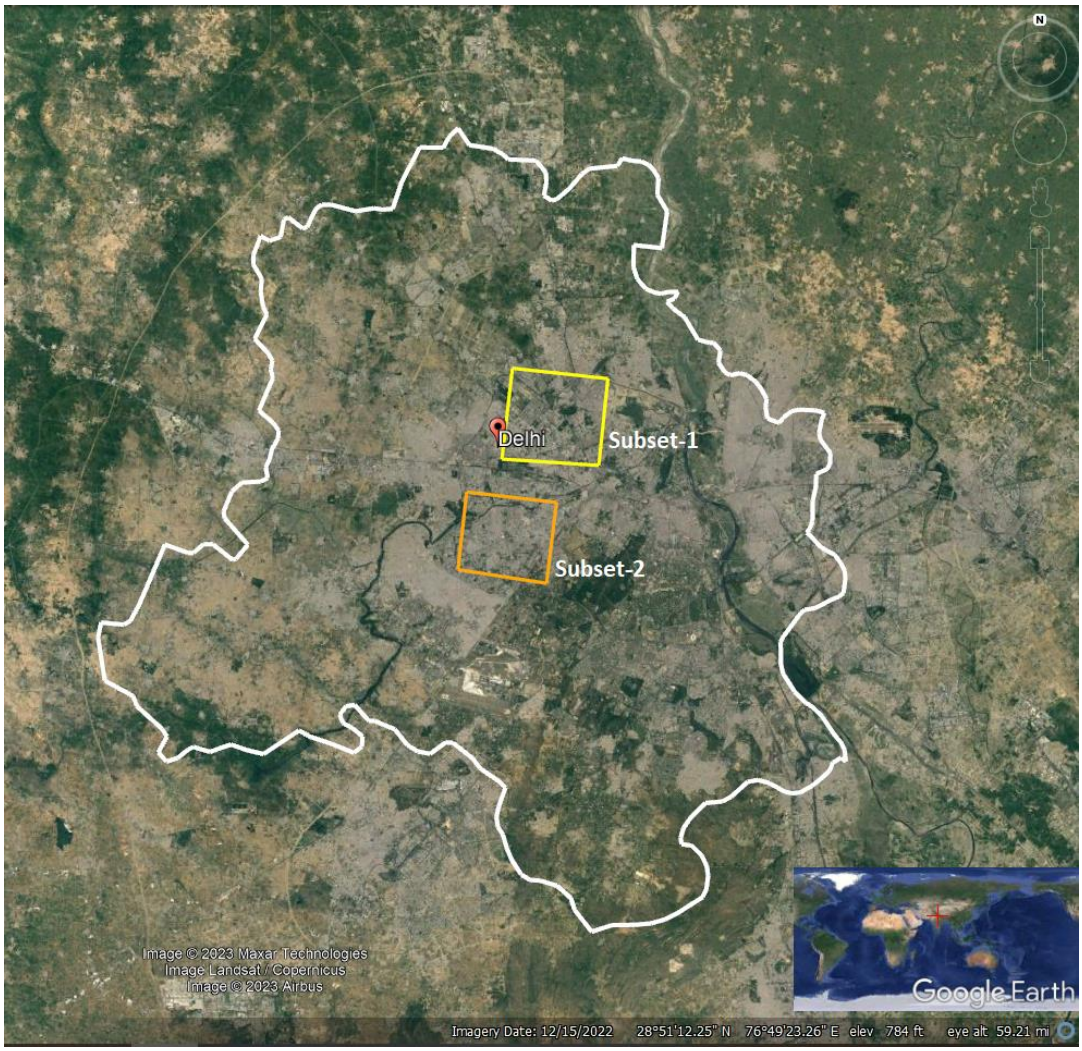


**Figure 3.1** Study Area in Delhi, India. *Source- Google earth.*

The metropolitan area of Delhi is increasingly seen to encompass surrounding satellite cities like Faridabad, Gurgaon, Ghaziabad, and Noida as well as areas beyond the NCT. According to the United Nations, this region, now known as the Central National Capital Region (CNCR), has approximately 26 million residents in 2016, making it the second-largest metropolitan area in the world [73].

In this study, two subsets are chosen (Fig. 3.1) within the urban setting of Delhi. The Subset 1 (Fig 3.3 (a,b)) mostly consists of well-built sectorial area which consist of sparse built-up with small region of dense built-up. It has parts of Rohini, Pitampura, Shalimar Bagh and Jhangirpuri etc. localities with total area of 43.5 sq. km. Subset 2 (Fig,3.3 (c,d)) on other hand consist of mostly dense urban built-up to less dense built-up of Tagore garden, Rajouri garden, Mayapuri, Ashok nagar etc. localities with total area of 38.14 sq. km. Both areas/subsets are chosen for comparing the performances of urban extraction and hyper-sharpening techniques on sparse to densely build/populated areas of the city.

## 3.2 DATA USED

For this study, the PRISMA sensor's hyperspectral and panchromatic data was used. The data was captured on 13 Dec 2022 over Delhi city. It had least cloud coverage of 0.39%. The Hyperspectral data was of 30 m spatial resolution with 234 bands and Panchromatic data was of 5 m spatial resolution with single band.

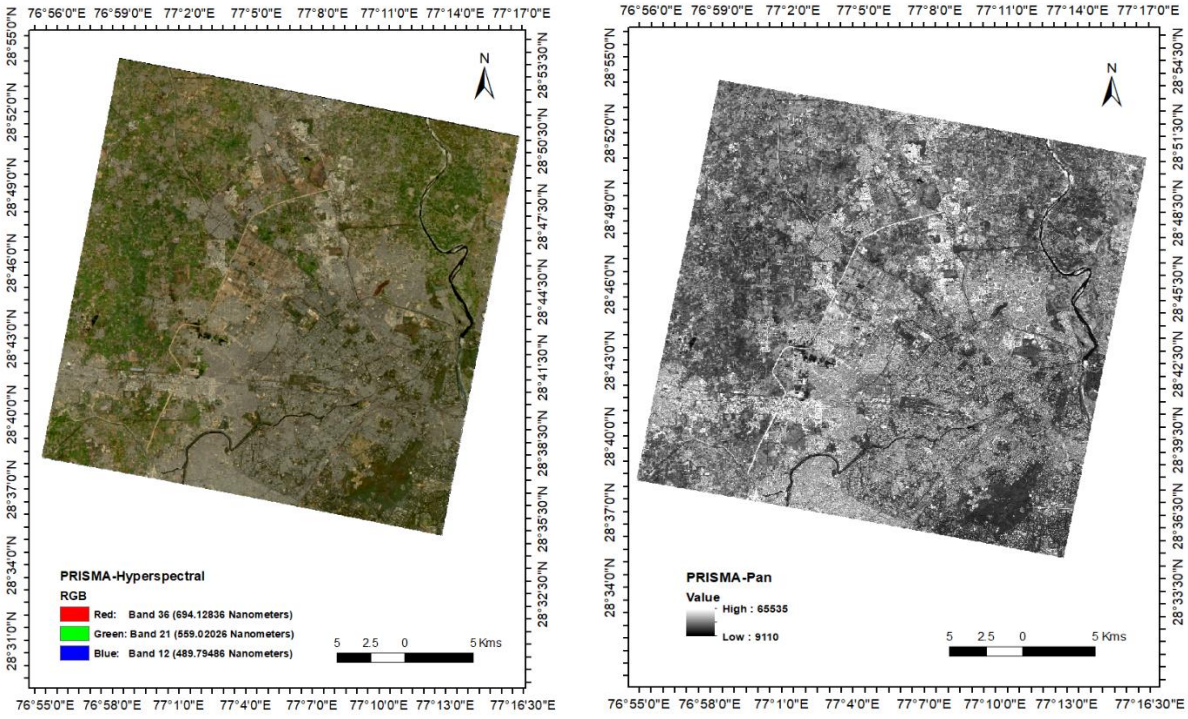


a. b.

**Figure. 3.2** (a) TCC of hyperspectral image of PRISMA sensor. (b) Panchromatic image of PRISMA sensor.

Both data were co-registered and covered 30×30 $km^2$ area. The received data was pre-processed up to processing level 2D that means geolocated and geocoded on-ground reflectance images. The data was further clipped to the extent of the two subsets of Delhi city.

### 3.21 PRISMA

The HYC (Hyperspectral Camera) and PAN (Panchromatic Camera) are two sensor modules that are part of the PRISMA satellite, an Italian spacecraft that was launched on March 22, 2019. The 237 channels of the HYC sensor's medium-resolution hyperspectral data are collected in the visible/near-infrared and near-infrared/shortwave infrared bands. It focuses on coastal areas, vegetation, inner seas, and high-resolution hyperspectral imagery of the land [74].

For fusion studies, the PAN module, a high-resolution optical imager, is co-registered with HYC. PRISMA uses a push broom scanning technology, offering a 30 km wide swath and a 1000 km wide field of sight on either side. Its Local Time on Descending Node (LTDN) is 10:30 a.m., and it is in a sun-synchronous orbit at a height of 614 km with an inclination of 98.19°. Its panchromatic camera has a wavelength range of 400–700 nm and a spatial resolution of one band of 5 m [74].

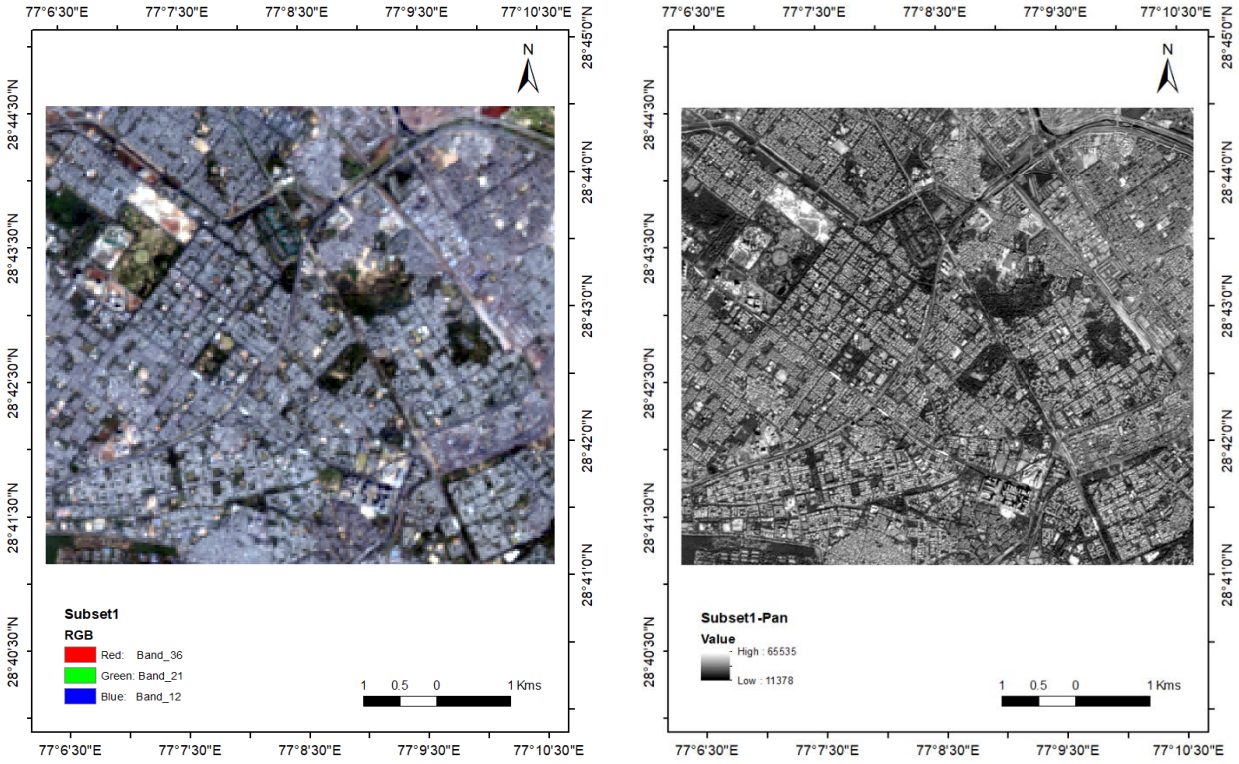


a. b.

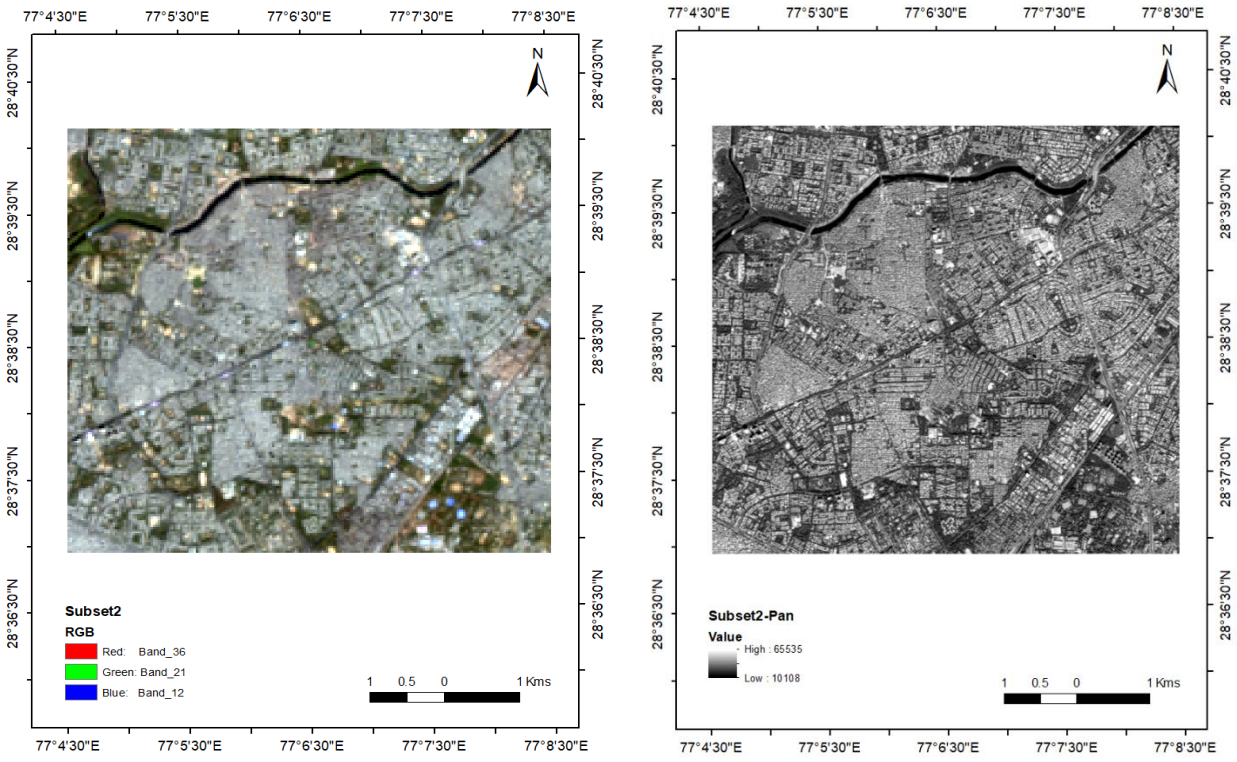


c. d.

**Figure. 3.3** (a) Subset 1-Hyperspectral image with 234 bands. (b) Subset 1-Panchromatic image of single band. (c) Subset 2-hyperspectral image of 234 bands. (d) Subset 2-Panchromatic image with single band.

The continuous spectral bands in the 400–2500 nm range are captured by the hyperspectral sensor, which has a spatial resolution of 30 meters. The spectral resolution of this sensor and the spectral sampling interval widths are both 12 nm. This sensor includes 66 bands in the visual near-infrared (VNIR) area of the light spectrum in the range of 400-1010 nm, and 173 bands in the short-wave infrared (SWIR) region between 920 and 2500 nm [75].

Numerous uses for PRISMA hyperspectral imagery (PHSI) have been discovered, including the mapping of forest fuels, the differentiation of different forest types, the mapping of burned areas, the prediction of methane emissions, agricultural use, the investigation of soil properties like moisture, organic matter, and carbon content, the assessment of water quality, and geological studies [75].

For the purpose of examining the accuracy of the areas extracted of different urban features the resultant areas were compared with high resolution multispectral

data. The data used was from PlanetScope sensor. DOVE CubeSat uses a PlanetScope camera with a 3m spatial resolution that operates in eight bands: red edge, red, green, green I, yellow, blue, coastal blue, and near infrared. We utilized Level-3B data, which had radiometric and sensor adjustments made as well as orthorectification and UTM projection [76].

**Table 3.1** Details of PlanetScope data. [76]

| | |
|---|---|
| **Revisit Time** | Daily at nadir |
| **Spectral Bands (nm)** | Coastal Blue: 431 - 452<br>Blue: 465 – 515<br>Green I: 513 - 549<br>Green: 547 – 583<br>Yellow: 600 - 620<br>Red: 650 – 680<br>Red Edge: 697 – 713<br>NIR: 845 – 885 |

## 3.3 METHODOLOGY

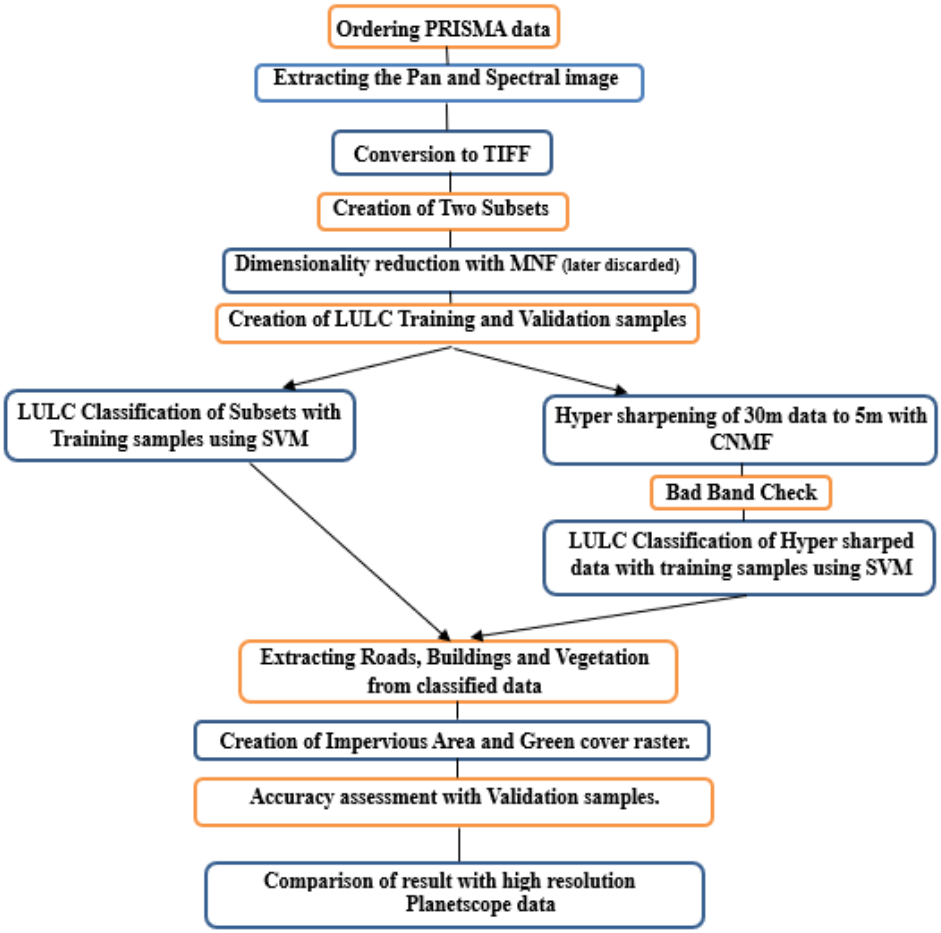


**Figure 3.4** Flowchart of the adopted methodology

### 3.3.1 Data Acquisition and Pre-processing.

The PRISMA data is owned by the Italian space agency ASI and can be accessed through their PRISMA portal. To obtain the data, registration and approval from ASI are required. The requested data was scheduled to be captured on December 13, 2022, and processed up to level 2d. The downloaded data was in he5 format, which can be opened in ENVI using IDL commands or in QGIS using the ENMAP-BOX plugin. The latest versions of ENVI, like 5.6, have built-in support for opening PRISMA data.

The data consisted of both panchromatic (PAN) and spectral images containing VNIR and SWIR bands. These images were exported to TIFF format. Two subsets named Subset 1 and Subset 2 were extracted over the city of Delhi. Both subsets exhibited a highly heterogeneous urban landscape with varying densities of buildings (high, medium, and low) of industrial, commercial, and residential nature. Additionally, there were wide to narrow roads, canals, lakes, parks, forests, croplands, and bare lands.

Subset 1 had a size of 231×210 pixels, while Subset 2 had 215×197 pixels, both covering an area of 30m each. Since each subset contained 234 bands, dimensionality reduction was necessary for improved classification results. Therefore, the MNF (Minimum Noise Fraction) technique, suitable for hyperspectral data, was chosen to reduce the dimensionality of the data.

#### 3.3.1.1 Minimum Noise Fraction

Minimum Noise Fraction (MNF) is a frequently used approach for decreasing noise and dimensionality in hyperspectral data processing. The MNF technique works by translating the original hyperspectral data into a collection of new orthogonal components called Minimum Noise Fraction components. The other components primarily represent noise, whereas these components are able to capture the majority of the signal information in the data. The dimensionality of the data can be decreased while still retaining the most crucial spectral information by choosing a subset of these components.[77]

The following stages make up the MNF algorithm: [78,79]

First, the mean of each spectral band is subtracted to center the data. The data is then whitened by being transformed to a new coordinate system where the covariance matrix is diagonal and the variance along each axis is equal to one, after the covariance matrix of the centered data has been determined. This step is essential because it removes correlations between spectral bands, which facilitates analysis of the data.

The MNF components are then extracted from the whitened data using an eigenvalue decomposition process. The amount of signal or noise that each component has been able to capture is shown by its eigenvalues. Most of the signal information in the data is included in the first few MNF components, whereas the latter components primarily represent noise. The interpretability and

physical significance of the MNF components are enhanced by rotating them to a new coordinate system.

Target detection, classification, and anomaly detection are just a few of the applications of hyperspectral data analysis where MNF has proved to be an efficient pre-processing method. It maintains the spectral information that is crucial for further analysis while reducing noise and improving the signal-to-noise ratio. Hyperspectral data, which might include hundreds or thousands of spectral bands, can be reduced in dimension by using MNF. The dimensionality of the data can be decreased without losing crucial spectral information by choosing a subset of the MNF components.

MNF was applied to both the datasets in ENVI. Forward MNF was estimated for full dataset. The first 29 bands for inverse MNF were selected from the result statistics and eigenvalues plot, bands showing constant 1 value were discarded and rest were used in the classification of the data.

### 3.3.2 Hyper-Sharpening

For extracting the urban features at higher resolution with more preciseness, there was a need to increase the resolution of our hyperspectral data from 30 m to higher spatial range.

Thus, the technique of Hyper-sharpening was employed. This technique fuses high resolution panchromatic image to low resolution hyperspectral image to provide a higher resolution hyperspectral image which can be used to better classify the data and extract required features. The hyper-sharpening algorithm that was used was easy to implement and most suited for hyper-sharpening hyperspectral data, called CNMF.

#### 3.3.2.1 Coupled Non-Negative Matrix Factorization (CNMF)

Coupled Non-Negative Matrix Factorization (CNMF) is an advanced technique used for hyper-sharpening, which involves fusing hyperspectral and multispectral data to generate images with enhanced spatial and spectral resolution. It assumes that the two datasets being fused are captured under similar atmospheric and illumination conditions, as well as being geometrically co-registered and radiometrically corrected.[65]

The CNMF algorithm operates through iterative steps to decompose the hyperspectral data into two nonnegative matrices: an endmember matrix and an abundance matrix. The endmember matrix captures the spectral signatures of the

materials present in the scene, while the abundance matrix represents the spatial details or the fraction of each material in each pixel.[65]

To achieve unmixing, a widely used method is the linear spectral mixture model, known as NMF (Non-Negative Matrix Factorization). NMF attempts to decompose a nonnegative data matrix into a product of nonnegative matrices. The CNMF algorithm performs two NMF unmixing steps in an alternating manner until convergence is reached.

During the iterations, CNMF capitalizes on the spectral information from the low-spatial-resolution hyperspectral data and the spatial information from the multispectral data. This approach helps to find an optimal initialization that leads to better local optima. Ultimately, the algorithm fuses the two matrices to generate a hyperspectral image with improved spectral-spatial resolution.[65]

In summary, CNMF leverages the strengths of both hyperspectral and multispectral data by iteratively decomposing the hyperspectral data into endmember and abundance matrices, exploiting the spectral and spatial information, and finally combining the matrices to produce a high-resolution hyperspectral image with enhanced spectral and spatial details. CNMF is particularly well-suited for scenes with complex spectral signatures. However, CNMF can be computationally expensive to compute and can be sensitive to noise in the data.[65]

In this thesis the PRISMA hyperspectral and Pan data of 30m and 5m resolution was used to hyper-sharp the spatial resolution of hyperspectral data from 30 m to 5m. It was done using MATLAB's Hyperspectral Imaging Library; a few lines of code were required for the process which is readily available on MathWorks website.

### 3.3.3 LULC Classification

The Land use and Land cover classification was done on all the datasets, raw PRISMA subsets of 30m, MNF outputs of both subsets and hyper-sharped images of both subsets for comparison. The classification method was also used for extracting the required features- Impervious surface area, Pervious surface area and urban green space from the classified images. The details of the classification process are mentioned below.

### 3.3.3.1 Sample creation

For Supervised classification of hyperspectral data, sample data of pixels representing different classes- Vegetation, Bare Land, Water, Roads, Buildings, need to be collected, these five classes of training samples were manually collected by observing the TCC (Bands: R=36, G=21, B=12) of hyperspectral image. Validation samples were collected by correlating the TCC image of PRISMA data to Google Earth imagery while collecting the samples.

Total 508 training samples were created for both the subsets. For Validation purpose total 1000 random and labelled points were generated from both the subsets. The table below gives the no. of Training and Testing sample pixels chosen for different classes in the two of the data. The total no. of pixels in area 1 data was 1384*1257 = 17,39,688 and for area 2 was 1286*1181 = 15,18,766.

**Table 3.2** Training and Testing sample pixels no. for different classes and both the areas

| CLASS | No. of Sample Pixels - 1 | | No. of Sample Pixels - 2 | |
|---|---|---|---|---|
| | Training | Test | Training | Test |
| **1. Vegetation** | 7812 | 5830 | 2277 | 2999 |
| **2. Bare-Land** | 5688 | 3569 | 725 | 157 |
| **3. Water** | 4896 | 1188 | 2547 | 1561 |
| **4. Roads** | 21744 | 4808 | 7139 | 687 |
| **5. Buildings** | 18435 | 14238 | 7155 | 1397 |
| *Total* | *58575* | *29633* | *19843* | *6801* |

### 3.3.3.2 Classification algorithm - Support Vector Machine (SVM)

The supervised machine learning approach known as Support Vector Machines (SVM) is frequently employed to address classification and regression issues. SVMs are quite good at handling difficult issues involving high-dimensional data. The SVM method searches for the best hyperplane that can most effectively split a set of labelled training data into distinct classes. The decision boundary dividing the data points is the hyperplane. [80]

The primary objective of the SVM method is to create a decision boundary that can accurately divide a multidimensional space into many categories. Hyperplanes are the limits of optimal decisions. The SVM approach selects the most crucial vectors or points, known as support vectors, that contribute to the hyperplane's creation.

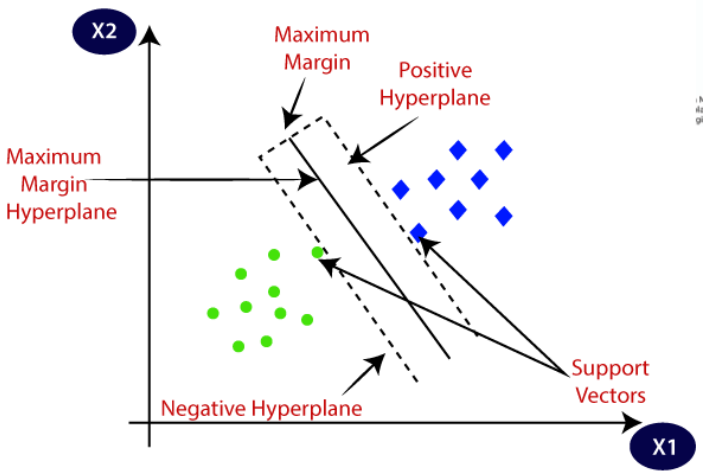


**Figure 3.5 A** Diagrammatic representation of SVM [82].

The SVM method chooses the most important vectors or points, referred to as support vectors, that help create the hyperplane. The data points with the greatest influence on the location of the hyperplane are these support vectors since they are situated closest to it. [80]

Finding the optimum hyperplane that optimizes the margin between the support vectors of various classes is the goal of linear SVM. The margin is the separation between the support vectors and the hyperplane along a perpendicular axis. The goal of SVM's formulation of this issue as an optimization problem is to maximize the margin while minimizing the classification error. Only linearly separable data may be handled by linear SVM. SVM uses the "kernel trick" to translate the input characteristics into a higher-dimensional space where linear separation is feasible when dealing with non-linearly separable data. The polynomial kernel, radial basis function (RBF) kernel, and sigmoid kernel are frequently used kernel functions. SVM may automatically work in the higher-dimensional space thanks to the kernel function, which eliminates the need to manually calculate the converted feature vectors.[81]

In SVM training, the best hyperplane to divide the classes is sought for. Through an optimization process, the training data, which consists of labelled instances, is utilized to learn the model parameters (weights and bias). The margin and regularization terms are part of a cost function that must be minimized in the optimization issue. Numerous strategies, including the Sequential Minimal Optimization (SMO) algorithm and gradient descent, can be used to solve the optimization. SVM foretells the class labels of previously unobserved data points during the classification phase. In order to map each data point to the feature space, the same transformation used during training is used. Depending on which side of the hyperplane the data point is on, the anticipated class is decided.[81]

The selection of the kernel function, regularization parameter (C), and kernel-specific parameters are only a few of the tuning factors for SVM. The trade-off between margin maximization and the penalty for misclassifications is influenced by these variables. To obtain optimal performance and avoid overfitting or underfitting, proper parameter adjustment is crucial. [80,81]

Due to its versatility in handling high-dimensional data, non-linear decision boundaries, and robustness against overfitting, SVMs have gained popularity across many industries. For big datasets, SVMs could be computationally costly. For SVM to work best, proper feature scale and parameter tweaking are essential. [81]

SVM was applied on all the datasets of both the subsets- raw subsets, MNF applied data, and Hyper-sharped data. The kernel function used was Radial Basis Function. The process was done using ENVI software.

## 3.4 Accuracy Assessment

Classification measures such as Precision, Recall, F-measure, Support, Confusion matrix and Cohen-kappa were used to find the accuracy of our classification and feature extraction outputs. Details about the measures being used is mentioned below [83].

### 3.4.1 Precision

Precision is the classifier's capacity to avoid classifying samples from one class as belonging to another or as positive when they are actually negative.

The ratio of the number of true positives to the number of false positives, or $t_p/t_p + f_p$ is used to measure accuracy. Intuitively, the classifier's precision is its capacity not to misclassify a negative sample as positive.

### 3.4.2 *F*- Measure

The accuracy and recall are the weighted harmonic means of the *F*-measure ($F_\beta \; and \; F_1$ measurements). A $F_\beta$ measure has a maximum value of 1 and a minimum value of 0. The recall and the accuracy are equally significant when $\beta$= 1, where are $F_1 and \; F_\beta$ are equivalent.

### 3.4.3 Recall

The ratio of the number of true positives to the number of false negatives, $t_p/t_p + f_n$, is known as the recall. The classifier's capacity to locate all of the correctly identified positive samples is known as recall.

### 3.4.4 Support

The amount of samples from each class in the validation samples constitutes the support.

### 3.4.5 Confusion matrix

By constructing the confusion matrix with each row representing the correct class, the confusion matrix function assesses classification accuracy.

Entry *i, j* in a confusion matrix is, by definition, the quantity of observations that actually belong in group *i* but were predicted to be in group *j*.

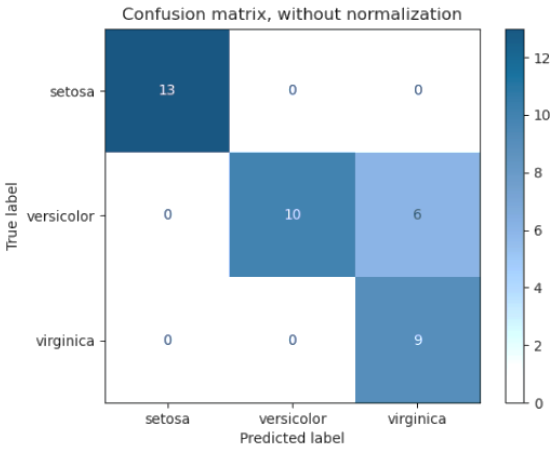


**Figure 3.6** An example depicting Confusion matrix [83].

### 3.4.6 Cohen-kappa Score

The cohen_kappa_score function is used to determine Cohen's kappa statistic. This measurement compares the annotations created by multiple human annotators, not a classifier to a ground truth.

Cohen's kappa calculates the degree of agreement between two raters who each assign N items to C categories that are mutually exclusive. Cohen's Kappa, in its simplest form, is a numerical measure of dependability for two raters who are assigning the same object the same rating, adjusted for the probability that the raters would agree by chance.

The kappa score is a value that ranges from -1 to 1. Good agreement is often defined as scores above 0.8, while zero or lower indicates no agreement (basically random labelling).

Therefore, if the likelihood of an agreement is equal to,

$$\kappa = \frac{p_0 - p_e}{p_0 - p_e}$$

then $p_0$ represents the model's overall accuracy and $p_e$ represents the measure of the agreement between the model's predictions and the actual class values as if it were a coincidence [83].

# CHAPTER 4

# OBSERVATIONS, RESULTS AND DISCUSSION

## 4.1 OBSERVATIONS

The steps of Data Acquisition, Pre-processing, Hyper-sharpening and Classification were followed using the data of two areas and following was observed:

### 4.1.1 Hyper-Sharpening using CNMF

The Hyper-sharpening of PRISMA hyperspectral image of 234 bands was done from 30 m to 5 m spatial resolution using coupled non negative factorization method, which resulted in a beautiful and detailed hyperspectral image at 5 m spatial resolution shown in the figure 4.1. For comparison, the raw subsets are kept along with the hyper-sharped data in the figure. As spatial enhancement could be observed by visual observation, spectral characteristics of the hyper-sharped data were also visualized for comparison with raw data. The spectra of both the subsets for both the raw and hyper-sharped data were visualized, vegetation spectra was chosen to find the effects of hyper-sharpening on the PRISMA data.

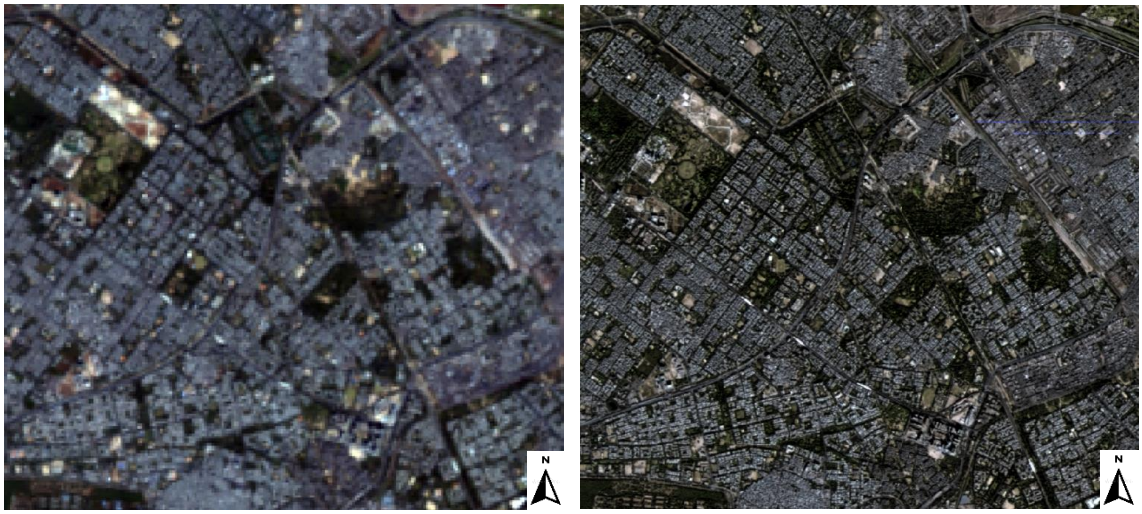

a. b.

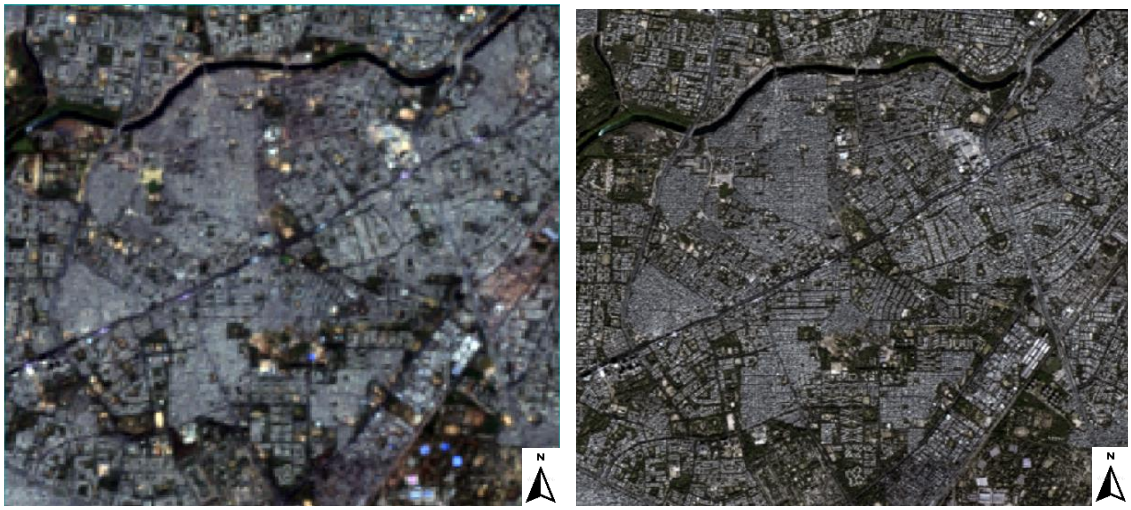

c. d.

**Figure 4.1** Hyper-Sharpening with CNMF results. (a) Raw 30m Subset 1 image. (b) Hyper-sharped 5m Subset1 image. (c) Raw 30m Subset 2 image. (d) Hyper-sharped 5m Subset2 image.

The Spectra were smoothened in ENVI for better visualization and were observed in its spectral viewer. Both the sharpened and raw spectra were seen as similar indicating the preserveness of spectral information in the hyper-sharped image. The spectra were similar, they were not exactly same, as before the curve smoothening process was applied, there were very slight deviations in the spectral curves of sharpened data in comparison to raw data which were smoothened by the process. The smoothened spectra of all the data are shown in the figure 4.2.

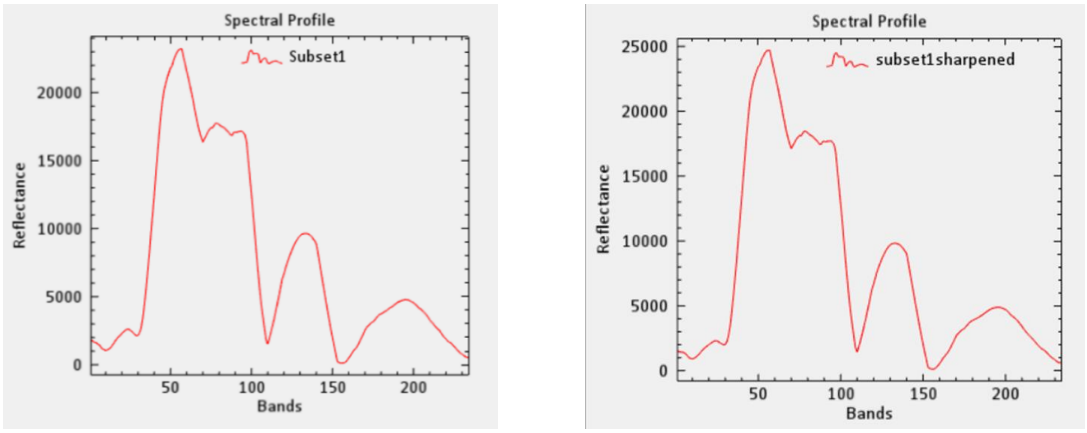


a. b.

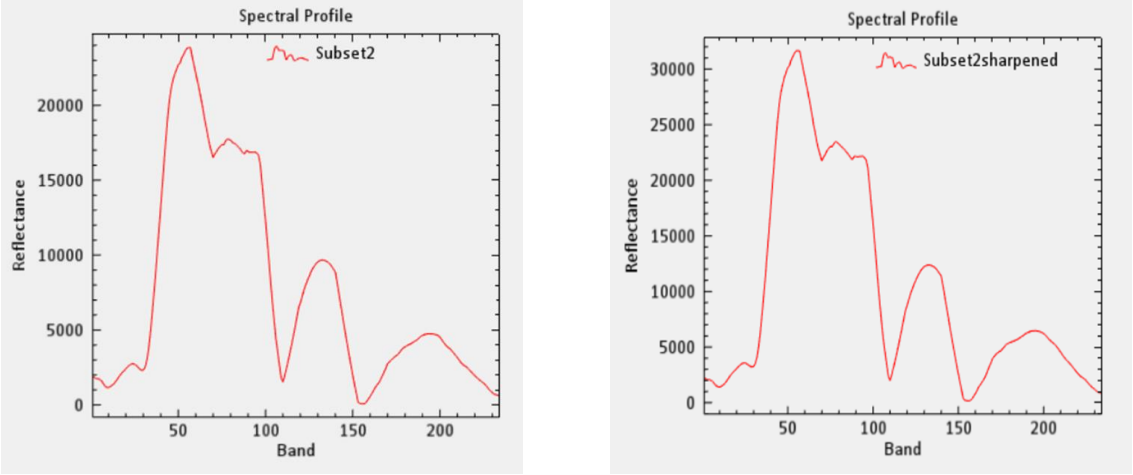


c. d.

**Figure 4.2** Spectral profile of a Vegetation pixel in (a) Raw 30m Subset 1 image. (b) Hyper-sharped 5m Subset1 image. (c) Raw 30m Subset 2 image. (d) Hyper-sharped 5m Subset2 image.

### 4.1.2 SVM Classification Outputs

The SVM classification algorithm was applied on raw 30 m data, hyper-sharped 5 m data and MNF outputs of both the areas of subset 1 and subset 2. The classification of MNF bands was poorer compared to raw subset and hyper-sharped data thus it was discarded and only raw data and hyper-sharped data was taken up to further processing. The Land cover and land use classification outputs are shown below in the figure 4.3.

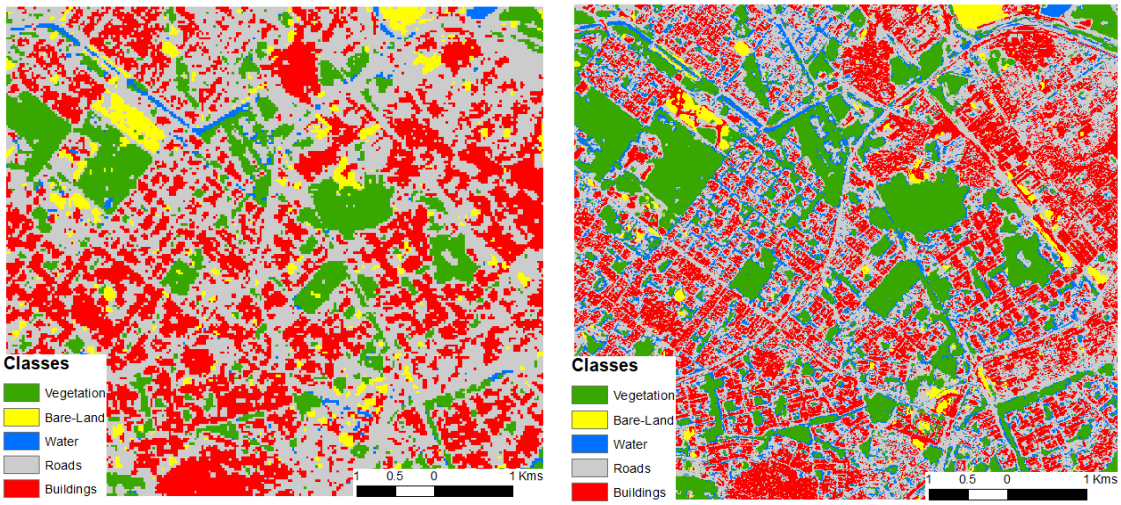


a. b.

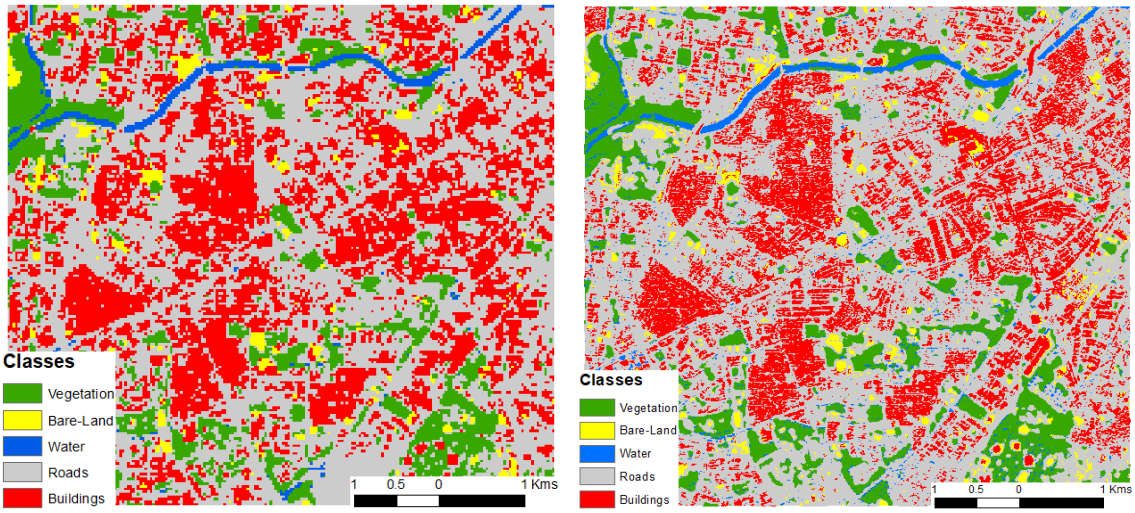


c. d.

**Figure 4.3** LCLU Classification results. (a) Raw 30m Subset 1 image. (b) Hyper-sharped 5m Subset1 image. (c) Raw 30m Subset 2 image. (d) Hyper-sharped 5m Subset2 image.

All classes such Roads, Buildings, Vegetation, Bare land, Water are segregated in the both the subsets, but in hyper-sharped version, visually it is seen that these features are better being distinguished such as roads in hyper-sharped subset 1, on comparing hyper-sharped and raw subset images the difference in the classification can be clearly seen. The classification in hyper-sharped images has more enhanced and is more detailed, obviously due to increased spatial resolution. So clearly classifying higher resolution data give better classification results than coarser data. Also, the difference in classification of highly dense and less dense built-up areas is also clearly seen in subset 1 and subset 2 areas. Features are more clearly classified in subset 1 urban area which has less dense built-up compared to denser built-up in area of subset 2.

The limitation that was observed in the classification of hyper-sharped images was that many dark pixels belonging to built-up area or vegetation are classified into water class due to hyper-sharpening process modifying the certain pixel/reflectance value to be lowest same as water.

## 4.2 RESULTS AND DISCUSSIONS

### 4.2.1 Extraction of Impervious-Pervious surface cover and Urban green space.

The classes that were selected for LULC classification were aimed at extracting features needed- Impervious area, Pervious area, and Urban green space. By combining binary rasters of road and building (outputs of classification) Impervious area map was created. By combining Bare land, Water and Vegetation's binary rasters, Pervious area map and by using Vegetation class's binary map created Urban Green space map was created.

The figure 4.4 depicts the maps that were resulted by extracting the required features using the hyper-sharped data for both the areas. All the maps depict the features better and in higher resolution comparison to the raw PRISMA images.

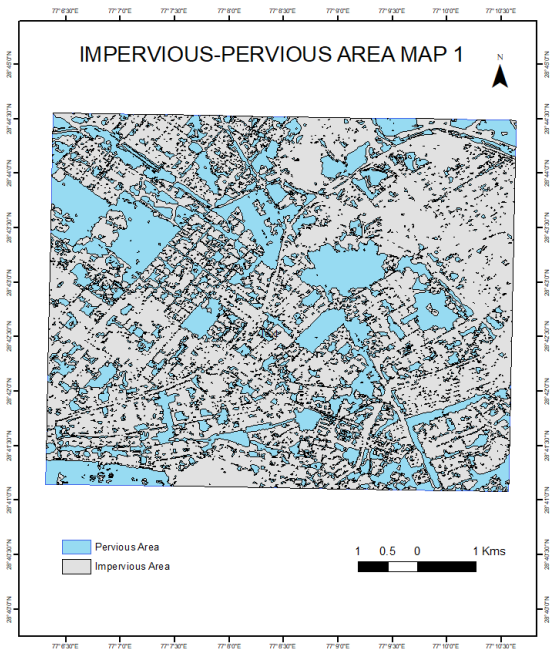


a.

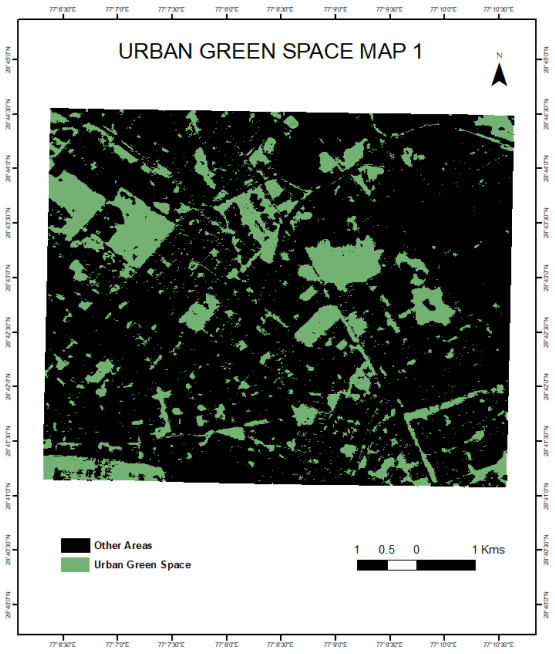


b.

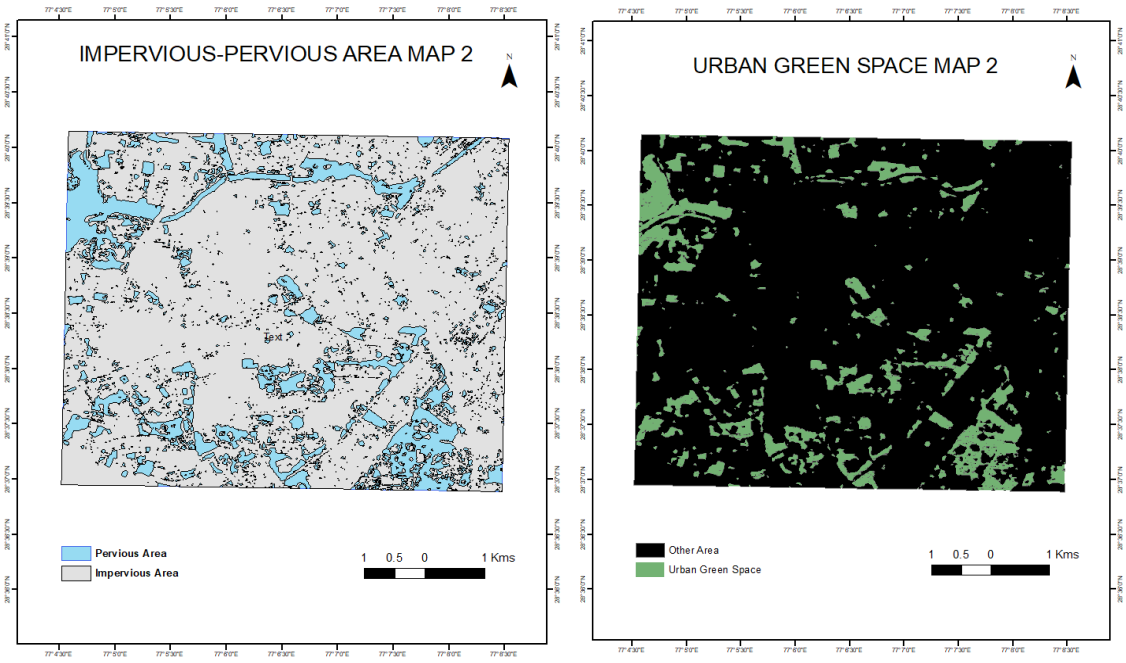


c. d.

**Figure 4.4** Features extracted maps from hyper-sharped images. (a) Impervious-Pervious area map for subset 1. (b) Urban Green Space for subset 2. (c) Impervious-Pervious area map for subset 2. (d) Urban Green Space for subset 2.

The Maps were created in ArcMap software of ArcGIS suite. Further they were used to calculate the areas of each feature in the above provided maps. The resultant areas are shown in Table 4.1. The differences in the areas of 30 m PRISMA image and 5 m hyper-sharper image even for same feature is clearly seen.

**Table 4.1** Areas of extracted features from different datasets in $Km^2$

| Data | Raw subset 1<br>At 30 m | Sharpened-Subset 1<br>At 5 m | Raw Subset 2<br>At 30 m | Sharpened Subset 2<br>At 5 m |
|---|---|---|---|---|
| Impervious Surface Area $km^2$ | 35.518018 | 29.590837 | 32.199973 | 31.520831 |
| Pervious area $km^2$ | 8.141447 | 14.069816 | 5.919933 | 6.62021 |
| Urban Green Space $km^2$ | 5.462073 | 8.636579 | 4.050981 | 4.41699 |

### 4.2.2 Classification Accuracy Assessment

For finding how accurate is the LULC classification, Verification samples that were collected earlier were used. Accuracy assessment points were created using classified image and verification samples in ArcMap, and by using Scikit-learn library of Python created the classification report.

The classification report talks about the accuracy of the SVM based LULC classification of hyper-sharped PRISMA data based on the parameters mentioned above. For Hyper-sharped image of Subset 1, it can be seen that the water pixels being most falsely classified and bare land most correctly based on their precision values.

Similarly in another area of hyper-sharped subset 2, Vegetation is most correctly classified class and bare land most falsely. The overall accuracy of hyper-sharped classified images for subset 1 is 87 % and for subset 2 is 92 %

Also, the Cohen kappa score for both classifications is above 0.8 which depicts good agreement. One thing to be noted here is that the verification of the images is done from the samples of same scale of 5 m as the hyper-sharped image. So, such accuracies could be produced.

The confusion matrix for both the images is also shown in the figure 4.5 and 4.6. It clearly depicts which samples are correctly classified into their classes and which are misclassified. Similarly, classification reports with confusion matrices for both the raw 30 m subsets are provided in Appendix 1 at the end of the report.

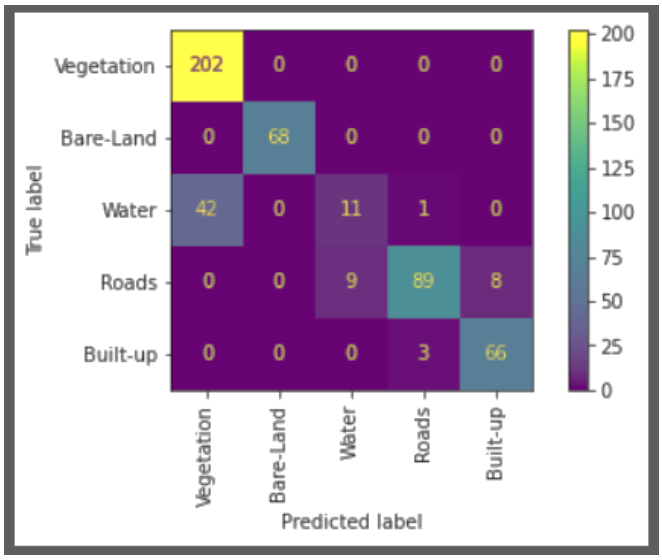


**Figure 4.5** Confusion matrix of Hyper-sharped Subset 1 classified image.

**Table 4.2** Classification report Hyper-sharped Subset 1 Image

| Classes/Measures | PRECISION | RECALL | F1 SCORE | SUPPORT |
|---|---|---|---|---|
| Vegetation | 0.83 | 1.00 | 0.91 | 202 |
| Bare-Land | 1.00 | 1.00 | 1.00 | 68 |
| Water | 0.55 | 0.20 | 0.30 | 54 |
| Roads | 0.96 | 0.84 | 0.89 | 106 |
| Built-up | 0.89 | 0.96 | 0.92 | 69 |
| Accuracy | | | | **0.87** |
| Cohen kappa score | | | | **0.8244184** |

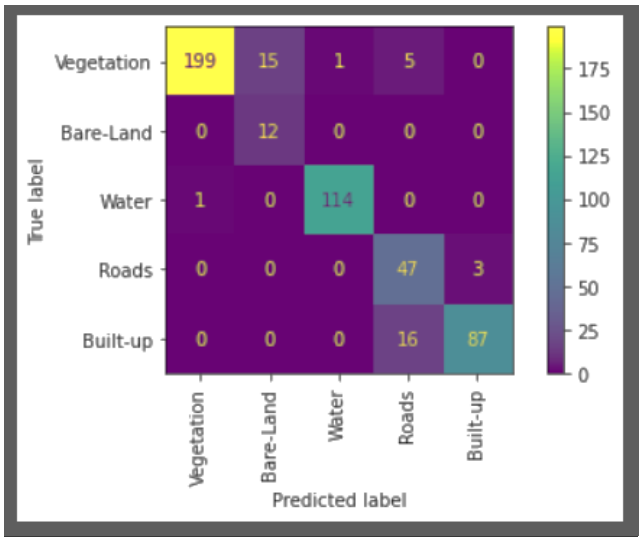


**Figure 4.6** Confusion matrix of Hyper-sharped Subset 2 classified image.

**Table 4.3** Classification report Hyper-sharped Subset 2 Image

| Classes/Measures | PRECISION | RECALL | F1 SCORE | SUPPORT |
|---|---|---|---|---|
| Vegetation | 0.99 | 0.90 | 0.95 | 220 |
| Bare-Land | 0.44 | 1.00 | 0.62 | 12 |
| Water | 0.99 | 0.99 | 0.99 | 115 |
| Roads | 0.69 | 0.94 | 0.80 | 50 |
| Built-up | 0.97 | 0.84 | 0.90 | 103 |
| Accuracy | | | | **0.92** |
| Cohen kappa score | | | | **0.8859723** |

### 4.2.3 Assessment of Extracted Areas.

As the accuracies of the LULC classification has been accessed, now to assess that how much the areas of the Hyper-sharped image extracted Urban features were close or similar to reality or outputs from other finer datasets, a comparison of areas of interest (Impervious surface area, Pervious surface area, and Urban Green space) extracted from hyperspectral PRISMA data hyper-sharped from 30 m to 5m was done to a multispectral 3m spatial resolution data of PlanetScope.

This high-resolution multispectral data for both subset regions was found up to an extent, so clipping of classified PRISMA data was done to that extent. The areas of required features were also noted. The PlanetScope data was also classified with SVM similar to hyper-sharped data to produce the required urban features and their areas. The result of the comparison is shown below in the able 4.4.

**Table 4.4** Comparison of Areas extracted from Hyper-sharped and PlanetScope Images

| Satellite data | *Prisma hyper-sharpened-5m* | *PlanetScope Image-3m* | | *Prisma hyper-sharpened-5m* | *PlanetScope Image-3m* | |
|---|---|---|---|---|---|---|
| **Urban Feature** | **Subset-1** | | **Accuracy %** | **Subset-2** | | **Accuracy %** |
| *Impervious Surface Area* $km^2$ | 28.888961 | 27.591537 | **95.3** | 19.087423 | 16.933176 | **87.3** |
| *Pervious area* $km^2$ | 13.377477 | 14.277901 | **93.7** | 3.788518 | 5.87534 | **64.5** |
| *Urban Green Space* $km^2$ | 8.640845 | 12.195111 | **70.9** | 2.557938 | 4.984575 | **51.4** |

Here in the table for subset 1, Impervious and Pervious surface areas are very close in no. and has accuracy of 95.3 and 93.7 percent depicting good results from sharpened data in respect to this feature in this area. For subset 2 the values differing

with accuracy of 87.3 and 64.5 percent, it seems like in less dense urban areas hyper-sharpening is more effective than compared calculating areas in dense urban areas.

In Urban Green space, the true values of areas are almost double with accuracies of this analysis being 70.9 and 51.4 percent, this large difference must be due to better spatial resolution of multispectral data which is better able to identify single trees or tree line as compared to the hyper-sharped PRISMA data. Also, along with the varying differences seen in areas of urban features, it should be noted that the hyper-sharped data was originally of 30 m spatial resolution and its hyper-sharped version is being compared to a multispectral 3 m data.

# CHAPTER 5

# CONCLUSIONS, RESEARCH CONTRIBUTION AND FUTURE SCOPE

## 5.1 CONCLUSION

Hyperspectral satellite data is both large in size and in opportunities it provides. In this work its potential has been used for monitoring one of largest and most populated Urban metropolitan area, Delhi, capital city of India. Satellite monitoring of urbanization is crucial for various applications such as in environmental, climatic and social. But the are lot of challenges urban centres produce such as their high heterogeneity of objects in really small space, which must be precisely captured for solving issues of urban people. Different urban materials, roofs, roads, vegetation, bare land, and waterways need accurate monitoring of their type and extent that could benefit in relation to monitoring pollution, analysing urban heat island effect, hydrological changes, monitoring urban expansion, socio-economic parameters, and urban ecology and thus impacts of humans on environment. Regular and timely monitoring of urban features leverages many applications to humans.

This study aimed on extracting features based on creating a high spectral- spatial resolution data's LULC, using that Impervious-Pervious surface area and Urban Green space of a part of the city were extracted, the Goal was to do it as efficiently as it can be done by utilizing the high Spectral-spatial resolution hyperspectral data for the purpose. It is known that hyperspectral data has power to capture variety of materials and characterize them better using its continuous and large spectral range. The problem is its spatial resolution that is too coarse for required application.

So, PRISMA hyperspectral data was Hyper-sharped from 30 m to 5 m using CNMF (Coupled Non-Negative Matrix Factorization) algorithm. It fuses spatial details from a high spatial resolution PAN data with spectral details from high spectral resolution hyperspectral data to create a High spatial-spectral resolution hyperspectral Image which now could be utilized for better extraction of the required urban features.

SVM classification was applied to the hyper-sharped image to get the LCLU, further by segregating and merging different classes, Impervious-Pervious maps, and Urban Green space maps were produced, plus the areas of these features were also

determined and had varying accuracies of 51.4 to 95.3 %. These results were satisfactory for Impervious-Pervious areas but need more work in calculating Urban Green space more accurately. Still, it is believed that higher spectral resolution improves the discrimination of features in urban areas and thus this data was chosen to work upon.

Thus, this study depicted that the methodology implemented here can be well utilized for extracting the urban features like Impervious-pervious areas in less dense cities at a good resolution of 5m.

The study also showed that for more dense urban areas, the need would be of a large-scale data of more than 5m pixel size for more accurate classification and feature extraction.

For Urban Green space, especially very high spatial resolution imageries that can capture signatures of single trees or tree lines will be required in urban areas for better calculation of vegetation.

## 5.2 RESEARCH CONTRIBUTION

The technique of Urban Feature extraction using Hyper-Sharpening could be employed anywhere in the world in any city for accessing latest variations in numbers of Impervious-Pervious area and Urban Green space at a good resolution of up to 5 m using freely available hyperspectral data.

These features aid as inputs in studying and monitoring urban environment, its socio-economic status and its climate.

This study also depicts the potential of hyperspectral data in characterizing urban features and help in their retrieval.

This Research also depicted one of the many urban applications of latest PRISMA data.

The accuracies attained in this study suggested a huge scope of improvement for the process of hyper-sharpening and feature extraction process.

## 5.3 FUTURE SCOPE

There is lot of work which can be done on using latest Hyper-sharpening algorithms and approaches to improve this study's results as it was seen in using CNMF, many pixels of water class were misclassified due to deterioration of dark pixels values, this can be avoided by using better and latest algorithms of hyper-sharpening such as Bayesian methods. Improving the hyper-sharpening results can significantly improve classification and thus improve the extraction of features and their areas. It can definitely increase the computation of Feature's areal accuracy.

Using very high-resolution multispectral data or high spatial resolution airborne hyperspectral data for such an analysis can be an easy option but its availability is an issue, as these images are usually priced or have limited access. Therefore, sharpening available images is fruitful for extracting urban features.

For improvement in the classification algorithm, SVM though is one the best ML algorithm for classifying hyperspectral data, techniques such as OBIA for high spatial resolution data can be used. Limitation is the requirement of high computational power to process high spatial resolution hyperspectral data for a regional scale and unavailability of open access software's.

Another group techniques that than can be used for improving hyperspectral sharpening or classification is Neural Networks and Deep learning. With more computational power, it can surely help in processing city scale data and extract their features.

Thus, whichever way is used, studying and mapping of features in the cities is crucial and can really help people in many ways. It also aids in monitoring human's impact over their environment and generate a balance between development and nature for a creating a better and sustainable future for all beings.

## REFERENCES


[1] T. M. Lillesand, R. W. Kiefer, and J. W. Chipman, "Remote sensing and image interpretation," John Wiley & Sons, 2015.

[2] M. Herold, S. V. Stehman, C. E. Woodcock, K. C. Seto, M. P. Lenney, and M. A. Wulder, "Accuracy assessment of land change detection: A review and update," *Remote Sensing of Environment*, vol. 115, no. 10, pp. 2420-2434, 2011.

[3] K. C. Seto, B. Güneralp, and L. R. Hutyra, "Global urban expansion and the future of biodiversity," *Science*, vol. 338, no. 6110, pp. 756-760, 2012.

[4] Angel, S., Parent, J., Civco, D. L., & Blei, A. (2011). The dimensions of urban expansion: A global assessment of urban land expansion from 1990 to 2000. *Environment and Urbanization*, 23(1), 167-186.

[5] J. R. &. M. Torrado, International Encyclopedia of Human Geography, Netherlands: *Elsevie*r, 2009, pp. 335-346.

[6] R. Navalgund, J. V and P. S. Roy, "Remote sensing applications: An overview," *Current Science*, vol. 93, no. 12, pp. 1747-1766, 2007.

[7] B. Waghmare and M. Suryawanshi, "A Review- Remote Sensing," *International Journal of Engineering Research and Applications*, vol. 7, no. 6, pp. 52-54, 2017.

[8] J. A. Benediktsson, J. Chanussot, and W. M. Moon, "Advances in Very-High-Resolution Remote Sensing," *Proceedings of the IEEE*, vol. 101, no. 3, pp. 566-569, 2013.

[9] Z. Zhang, Y. Wu, and X. Li, "A Survey of Urban Feature Extraction from Remote Sensing Images," 2016.

[10] Y. Wang, Y. Wu, and Z. Zhang, "A Review of Methods for Urban Feature Extraction from Remote Sensing Images," 2017.

[11] L. Li, Y. Wu, and Z. Zhang, "A Comparative Study of Methods for Urban Feature Extraction from Remote Sensing Images," 2018.

[12] Z. Zhang, Y. Wu, and X. Li, "Challenges and Opportunities of Urban Feature Extraction from Remote Sensing Images," 2016.

[13] P. Song, X. Li, C. Wu, C. Zhang, and L. Shi, "A review of remote sensing image fusion methods," *ISPRS Journal of Photogrammetry and Remote Sensing*, vol. 100, pp. 16-28, 2015.

[14] X. Huang, L. Zhang, and S. Li, "A Review of Multispectral and Panchromatic Image Fusion Methods," *Information Fusion*, vol. 48, pp. 35-60, 2019.

[15] B. Salehi, D. Akbari, M. Shokri, and A. M. Alimi, "A comparative analysis of pixel-based and feature-based fusion methods for remote sensing images," *International Journal of Applied Earth Observation and Geoinformation*, vol. 52, pp. 502-513, 2016.

[16] C. Pohl and J. L. Van Genderen, "Multisensor image fusion in remote sensing: concepts, methods, and applications," *International Journal of Remote Sensing*, vol. 19, no. 5, pp. 823-854, 1998.

[17] P. P. Singh and R. D. Garg, "Automatic road extraction from high resolution satellite image using adaptive global thresholding and morphological operations," *Journal of the Indian Society of Remote Sensing*, vol. 41, pp. 631-640, 2013.

[18] D. Lu, G. Li, W. Kuang, and E. Moran, "Methods to extract impervious surface areas from satellite images," *International Journal of Digital Earth*, vol. 7, no. 2, pp. 93-112, 2014.

[19] Aishwarya et al., "A technique to extract urban built-up, land/vegetation and water features from Enhanced Thematic Mapper," 2017.

[20] H. Fang, Y. Wei, and Q. Dai, "A novel remote sensing index for extracting impervious surface distribution from Landsat 8 OLI imagery," *Applied Sciences*, vol. 9, no. 13, p. 2631, 2019.

[21]

[22] Y. Cao, Y. Xun, Y. Han, J. Chen, S. Wang, Z. Zhang, N. Du, and H. Meng, "Feature Extraction of Remote Sensing Images Based on Bat Algorithm and Normalized Chromatic Aberration," IFAC-PapersOnLine, vol. 52, no. 24, pp. 318-323, 2019.

[23] S. I. Deliry, Z. Y. Avdan, and U. Avdan, "Extracting urban impervious surfaces from Sentinel-2 and Landsat-8 satellite data for urban planning and environmental management," Environmental Science and Pollution Research, vol. 28, no. 6, pp. 6572-6586, 2021.

[24] X. Ma, Q. Man, X. Yang, P. Dong, Z. Yang, J. Wu, and C. Liu, "Urban Feature Extraction within a Complex Urban Area with an Improved 3D-CNN Using Airborne Hyperspectral Data," *Remote Sensing*, vol. 15, no. 4, p. 992, 2023.

[25] W. Li, J. D. M. Saphores, and T. W. Gillespie, "A comparison of the economic benefits of urban green spaces estimated with NDVI and with high-resolution land cover data," *Landscape and Urban Planning*, vol. 133, pp. 105-117, 2015.

[26] Aram, E. H. García, E. Solgi, and S. Mansournia, "Urban green space cooling effect in cities," *Heliyon*, vol. 5, no. 4, p. e01339, 2019.

[27] Huang, J. Yang, N. Clinton, L. Yu, H. Huang, I. Dronova, and J. Jin, "Mapping the maximum extents of urban green spaces in 1039 cities using dense satellite images," *Environmental Research Letters*, vol. 16, no. 6, p. 064072, 2021.

[28] S. E. Jozdani, B. A. Johnson, and D. Chen, "Comparing deep neural networks, ensemble classifiers, and support vector machine algorithms for object-based urban land use/land cover classification," *Remote Sensing*, vol. 11, no. 14, p. 1713, 2019.

[29] M. A. Moharram and D. M. Sundaram, "Land Use and Land Cover Classification with Hyperspectral Data: A comprehensive review of methods, challenges and future directions," *Neurocomputing*, 2023.

[30] P. Gamba, A. Villa, A. Plaza, J. Chanussot, and J. A. Benediktsson, "Urban area product simulation for the EnMap hyperspectral sensor," in 2011 IEEE *International Geoscience and Remote Sensing Symposium*, 2011, pp. 1259-1262.

[31] S. Dobhal, "Performance analysis of high-resolution and hyperspectral data fusion for classification and linear feature extraction," ITC, January 2008.

[32] L. Loncan, L. B. Almeida, J. M. Bioucas-Dias, X. Briottet, J. Chanussot, N. Dobigeon, S. Fabre, W. Liao, G. A. Licciardi, M. Simoes et al., "Hyperspectral Pansharpening: A Review," *IEEE Geoscience and Remote Sensing Magazine*, vol. 3, no. 3, pp. 27-46, 2015.

[33] Mookambiga and V. Gomathi, "Comprehensive review on fusion techniques for spatial information enhancement in hyperspectral imagery," *Multidimensional Systems and Signal Processing*, vol. 27, pp. 863-889, 2016.

[34] M. Selva, B. Aiazzi, F. Butera, L. Chiarantini, and S. Baronti, "Hyper-sharpening: A first approach on SIM-GA data," *IEEE Journal of Selected Topics in Applied Earth Observations and Remote Sensing*, vol. 8, no. 6, pp. 3008-3024, 2015.

[35] X. Lu, J. Zhang, X. Yu, W. Tang, T. Li, and Y. Zhang, "Hyper-sharpening based on spectral modulation," *IEEE Journal of Selected Topics in Applied Earth Observations and Remote Sensing*, vol. 12, no. 5, pp. 1534-1548, 2019.

[36] N. Yokoya, T. Yairi, and A. Iwasaki, "Coupled nonnegative matrix factorization unmixing for hyperspectral and multispectral data fusion,"

*IEEE Transactions on Geoscience and Remote Sensing*, vol. 50, no. 2, pp. 528-537, 2011.

[37] J. R. Jensen, "Introductory digital image processing: a remote sensing perspective," Prentice Hall, 2005.

[38] D. Lu and Q. Weng, "A survey of image classification methods and techniques for improving classification performance," *International Journal of Remote Sensing*, vol. 28, no. 5, pp. 823-870, 2007.

[39] J. A. Richards and X. Jia, "Remote sensing digital image analysis: an introduction," *Springer Science & Business Media*, 2006.

[40] P. Wang and H. Liu, "Mapping impervious surface area in an urban area by integrating spectral, spatial, and contextual information using machine learning algorithms," *Remote Sensing*, vol. 8, no. 10, p. 819, 2016.

[41] C. Wu and A. T. Murray, "Estimating impervious surface distribution by spectral mixture analysis," *Remote Sensing of Environment*, vol. 84, no. 4, pp. 493-505, 2003.

[42] G. Xian, C. Homer, J. Dewitz, J. Fry, N. Hossain, and J. Wickham, "The change of impervious surface area between 2001 and 2006 in the conterminous United States," *Photogrammetric Engineering & Remote Sensing*, vol. 77, no. 8, pp. 758-762, 2011.

[43] M. Metzger, "Fractal analysis of satellite images: A new approach to land cover classification," New York: *Springer*-Verlag, 2000.

[44] R. M. Haralick, K. Shanmugam, and I. Dinstein, "Textural features for image classification," *IEEE Transactions on Systems, Man, and Cybernetics*, vol. SMC-3, no. 6, pp. 610-621, 1973.

[45] J. Benz, P. Hofmann, and G. Willhauck, "Fractal analysis of topographic surfaces," in Proceedings of the 1994 *IEEE International Geoscience and Remote Sensing Symposium* (IGARSS '94), vol. 3, pp. 1491-1493, 1994.

[46] C. E. Woodcock, K. C. Seto, M. P. Lenney, S. A. Macomber, and W. C. Seto, "Classification and change detection using Landsat TM data: When and how to correct atmospheric effects?," *Remote Sensing of Environment*, vol. 75, no. 2, pp. 230-244, 2001.

[47] N. Zhao, S. Chen, C. Wang, and Q. Liu, "An object-based approach for impervious surface extraction using ZY-3 multispectral imagery," *Remote Sensing*, vol. 7, no. 7, pp. 8170-8194, 2015.

[48] Y. Liu, X. Zhang, W. Zhang, and X. Li, "Urban green space extraction from high-resolution satellite images using deep learning," *Remote Sensing*, vol. 9, no. 9, p. 917, 2017.

[49] W. Jiang, X. Li, J. Yang, and H. Luan, "The potential of sentinel-2 spectral configuration for urban green space extraction," *Remote Sensing*, vol. 9, no. 8, p. 809, 2017.

[50] L. Wang, Q. Xin, and J. Zhang, "Mapping urban green space with high-resolution imagery and deep learning," *Remote Sensing*, vol. 11, no. 19, p. 2295, 2019.

[51] F. Yuan, M. E. Bauer, and A. B. Jannetta, "A comparison of impervious surface area and normalized difference vegetation index as indicators of surface urban heat island effects in Landsat imagery," *Remote Sensing of Environment*, vol. 114, no. 7, pp. 1474-1481, 2010.

[52] X. Yu, X. Guo, and Y. Wu, "Mapping urban green space using high-resolution remote sensing imagery and landscape metrics," *International Journal of Environmental Research and Public Health*, vol. 16, no. 14, p. 2473, 2019.

[53] E. F. Lambin and H. J. Geist (Eds.), "Land-use and land-cover change: local processes and global impacts," *Springer* Science & Business Media, 2006.

[54] M. Herold, J. Scepan, and K. C. Clarke, "The use of remote sensing and landscape metrics to describe structures and changes in urban land uses," *Environment and Planning* A, vol. 34, no. 8, pp. 1443-1458, 2002.

[55] T. M. Lillesand, R. W. Kiefer, and J. W. Chipman, "Remote sensing and image interpretation," *John Wiley & Sons*, 2015.

[56] Q. Weng and D. Lu, "A sub-pixel analysis of urban land use/cover from DMSP/OLS nightlights," *Remote sensing of Environment*, vol. 112, no. 11, pp. 5049-5063, 2008.

[57] G. M. Foody, "Status of land cover classification accuracy assessment," *Remote sensing of Environment*, vol. 80, no. 1, pp. 185-201, 2002.

[58] D. Lu and Q. Weng, "A survey of image classification methods and techniques for improving classification performance," *International Journal of Remote Sensing*, vol. 28, no. 5, pp. 823-870, 2007.

[59] R. G. Congalton and K. Green, "Assessing the accuracy of remotely sensed data: principles and practices," CRC press, 2009.

[60] L. Li, W. Li, J. Li, and X. Zhang, "A review of supervised object-based land-cover image classification," *ISPRS Journal of Photogrammetry and Remote Sensing*, vol. 103, pp. 97-110, 2015.

[61] Gómez, J. C. White, and M. A. Wulder, "Optical and SAR sensor synergies for forest and land cover mapping in a western Canadian test site," *Remote Sensing*, vol. 8, no. 3, p. 218, 2016.

[62] Q. Du, L. Fang, and Y. Feng, "A novel hyperspectral and panchromatic image fusion method using non-local low-rank matrix recovery," *Remote Sensing*, vol. 11, no. 14, p. 1659, 2019.

[63] Y. Li, Q. Chen, Q. Du, X. Liu, and C. Wang, "Hyperspectral and panchromatic image fusion based on compressive sensing and principal component analysis," *Remote Sensing*, vol. 11, no. 10, p. 1151, 2019. [Online]. Available: https://doi.org/10.3390/rs11101151

[64] Plaza et al., "Recent advances in techniques for hyperspectral image processing," *Remote Sensing of Environment*, vol. 113, Supplement 1, pp. S110-S122, 2009. [Online]. Available: https://doi.org/10.1016/j.rse.2008.10.008

[65] D. Tuia, G. Moser, and L. Bruzzone, "A novel pansharpening method based on the a trous wavelet transform," *IEEE Transactions on Geoscience and Remote Sensing*, vol. 49, no. 6, pp. 2191-2200, 2011. [Online]. Available: https://doi.org/10.1109/TGRS.2011.2106849

[66] N. Yokoya, T. Yairi, and A. Iwasaki, "Coupled nonnegative matrix factorization unmixing for hyperspectral and multispectral data fusion," *IEEE Transactions on Geoscience and Remote Sensing*, vol. 50, no. 2, pp. 528-537, 2011.

[67] G. Vivone et al., "A critical comparison among pansharpening algorithms," *IEEE Transactions on Geoscience and Remote Sensing*, vol. 53, no. 5, pp. 2565-2586, 2015. [Online]. Available: https://doi.org/10.1109/TGRS.2014.2360446

[68] D. A. Landgrebe and Q. Du, "Recent advances in hyperspectral image processing," *IEEE Signal Processing Magazine*, vol. 20, no. 3, pp. 17-28, 2003.

[69] Plaza, J. A. Benediktsson, and J. W. Boardman, "Recent advances in techniques for hyperspectral image processing," *Remote Sensing of Environment*, vol. 113, Supplement, pp. S110-S122, 2009.

[70] M. Bioucas-Dias and A. Plaza, "Hyperspectral image processing: A review," *IEEE Geoscience and Remote Sensing Magazine*, vol. 1, no. 2, pp. 6-36, 2012.

[71] Mookambiga and V. Gomathi, "Comprehensive review on fusion techniques for spatial information enhancement in hyperspectral imagery," *Multidimensional Systems and Signal Processing*, vol. 27, pp. 863-889, 2016.

[72] M. Selva et al., "Hyper-sharpening: A first approach on SIM-GA data," *IEEE Journal of Selected Topics in Applied Earth Observations and Remote Sensing*, vol. 8, no. 6, pp. 3008-3024, 2015.

[73] X. Lu et al., "Hyper-sharpening based on spectral modulation," *IEEE Journal of Selected Topics in Applied Earth Observations and Remote Sensing*, vol. 12, no. 5, pp. 1534-1548, 2019.

[74] National Bureau of Soil Survey and Land Use Planning, "Soil Survey and Land Use Plan of Delhi Territory," 1979.

[75] E. Vangi, G. D'Amico, S. Francini, F. Giannetti, B. Lasserre, M. Marchetti, and G. Chirici, "The new hyperspectral satellite PRISMA: Imagery for forest types discrimination," *Sensors*, vol. 21, no. 4, p. 1182, 2021. [Online].

[76] https://www.eoportal.org/satellite-missions/prisma-hyperspectral#eop-quick-facts-section

[77] "PlanetScope," Earth Online (ESA), [Online]. Available: https://earth.esa.int/eogateway/missions/planetscope

[78] Green, M. Berman, P. Switzer, and M. D. Craig, "A transformation for ordering multispectral data in terms of image quality with implications for noise removal," *IEEE Transactions on Geoscience and Remote Sensing*, vol. 26, no. 1, pp. 65-74, 1988.

[79] M. E. Winter, "Noise-adjusted principal components analysis for hyperspectral image classification," *Journal of Electronic Imaging*, vol. 8, no. 4, pp. 410-421, 1999.

[80] D. Manolakis and G. Shaw, "Detection algorithms for hyperspectral imaging applications," *IEEE Signal Processing Magazine*, vol. 19, no. 1, pp. 29-43, 2002.

[81] M. Bishop, "Pattern Recognition and Machine Learning."

[82] S. Abe, "Support Vector Machines for Pattern Classification."

[83] "Machine Learning - Support Vector Machine Algorithm," JavaTpoint, [Online]. Available: https://www.javatpoint.com/machine-learning-support-vector-machine-algorithm.

[84] "classification_report - scikit-learn 0.24.2 documentation," scikit-learn.org, [Online]. Available: https://scikit-learn.org/stable/modules/generated/sklearn.metrics.classification_report.html#sklearn.metrics.classification_report.

## Appendix 1:

- **LULC Classification report for Raw 30 m PRISMA hyperspectral data**

### 1. Subset 1.

| | precision | recall | f1-score | support |
|---|---|---|---|---|
| Vegetation | 0.87 | 0.91 | 0.89 | 137 |
| Bare-Land | 0.85 | 0.79 | 0.82 | 43 |
| Water | 0.70 | 0.33 | 0.45 | 21 |
| Roads | 0.58 | 0.85 | 0.69 | 119 |
| Built-up | 0.94 | 0.78 | 0.85 | 280 |
| accuracy | | | 0.81 | 600 |
| macro avg | 0.79 | 0.73 | 0.74 | 600 |
| weighted avg | 0.84 | 0.81 | 0.81 | 600 |

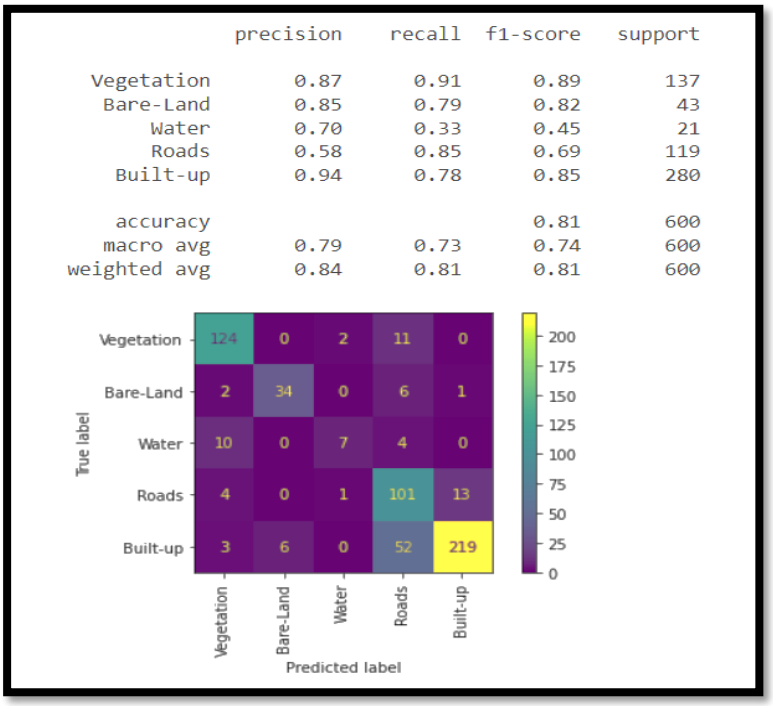


### 2. Subset 2

| | precision | recall | f1-score | support |
|---|---|---|---|---|
| Vegetation | 0.98 | 0.90 | 0.94 | 220 |
| Bare-Land | 0.23 | 0.50 | 0.32 | 12 |
| Water | 1.00 | 0.97 | 0.98 | 115 |
| Roads | 0.63 | 0.94 | 0.75 | 50 |
| Built-up | 0.94 | 0.78 | 0.85 | 103 |
| accuracy | | | 0.89 | 500 |
| macro avg | 0.76 | 0.82 | 0.77 | 500 |
| weighted avg | 0.92 | 0.89 | 0.90 | 500 |